Available online at www.sciencedirect.com

ScienceDirect

Geochimica et Cosmochimica Acta 188 (2016) 73–92

Geochimica et Cosmochimica Acta

www.elsevier.com/locate/gca

Study of thermochemical sulfate reduction mechanism using compound specific sulfur isotope analysis

Alexander Meshoulam [a], Geoffrey S. Ellis [b], Ward Said Ahmad [a], Andrei Deev [c], Alex L. Sessions [d], Yongchun Tang [c], Jess F. Adkins [d], Liu Jinzhong [e], William P. Gilhooly III [f], Zeev Aizenshtat [g], Alon Amrani [a,*]

[a] *Institute of Earth Sciences, Hebrew University, Jerusalem 91904, Israel*
[b] *U.S. Geological Survey, Denver, CO 80225, USA*
[c] *Power, Environmental and Energy Research Institute (PEERi), Covina, CA 91722, USA*
[d] *Division of Geological and Planetary Sciences, California Institute of Technology, Pasadena, CA 91125, USA*
[e] *Guangzhou Institute of Geochemistry, Chinese Academy of Sciences, Guangzhou 510640, China*
[f] *Department of Earth Sciences Indiana University-Purdue University Indianapolis, IN 46202, USA*
[g] *Institute of Chemistry, Hebrew University, Jerusalem 91904, Israel*

Received 26 November 2015; accepted in revised form 13 May 2016; Available online 26 May 2016

Abstract

The sulfur isotopic fractionation associated with the formation of organic sulfur compounds (OSCs) during thermochemical sulfate reduction (TSR) was studied using gold-tube pyrolysis experiments to simulate TSR. The reactants used included *n*-hexadecane (*n*-C_{16}) as a model organic compound with sulfate, sulfite, or elemental sulfur as the sulfur source. At the end of each experiment, the S-isotopic composition and concentration of remaining sulfate, H_2S, benzothiophene, dibenzothiophene, and 2-phenylthiophene (PT) were measured. The observed S-isotopic fractionations between sulfate and BT, DBT, and H_2S in experimental simulations of TSR correlate well with a multi-stage model of the overall TSR process. Large kinetic isotope fractionations occur during the first, uncatalyzed stage of TSR, 12.4‰ for H_2S and as much as 22.2‰ for BT. The fractionations decrease as the H_2S concentration increases and the reaction enters the second, catalyzed stage. Once all of the oxidizable hydrocarbons have been consumed, sulfate reduction ceases and equilibrium partitioning then dictates the fractionation between H_2S and sulfate (~17‰).

Experiments involving sparingly soluble $CaSO_4$ show that during the second catalytic phase of TSR the rate of sulfate reduction exceeds that of sulfate dissolution. In this case, there is no apparent isotopic fractionation between source sulfate and generated H_2S, as all of the available sulfate is effectively reduced at all reaction times. When $CaSO_4$ is replaced with fully soluble Na_2SO_4, sulfate dissolution is no longer rate limiting and significant S-isotopic fractionation is observed. This supports the notion that $CaSO_4$ dissolution can lead to the apparent lack of fractionation between H_2S and sulfate produced by TSR in nature. The S-isotopic composition of individual OSCs record information related to geochemical reactions that cannot be discerned from the $\delta^{34}S$ values obtained from bulk phases such as H_2S, oil, and sulfate minerals, and provide important mechanistic details about the overall TSR process.

Keywords: Thermochemical alteration; Organic matter; Sulfur compounds; Sulfate dissolution; Isotopes

* Corresponding author. Tel.: +972 2 6585477; fax: +972 25662581.
E-mail address: alon.amrani@mail.huji.ac.il (A. Amrani).

http://dx.doi.org/10.1016/j.gca.2016.05.026
0016-7037/

1. INTRODUCTION

Thermochemical sulfate reduction (TSR) involves a complex reaction network that ultimately results in oxidation of organic carbon (OC) to CO_2 and reduction of sulfate to H_2S (Machel et al., 1995; Worden and Smalley, 2001). Experimental and field observations have shown that TSR is a kinetically controlled process with an onset temperature between 100 and 140 °C, and that temperature is the most critical factor controlling the rate and extent of TSR (Machel, 1987, 2001; Heydari and Moore, 1989; Goldstein and Aizenshtat, 1994; Goldhaber and Orr, 1995; Worden et al., 1995 and references therein).

In one of the first laboratory simulations of TSR, Toland (1960) noted that organic compounds were not oxidized when only sulfate was present; however, the presence of even minute amounts of H_2S (or other reduced sulfur species) were able to initiate sulfate reduction. Subsequent studies supported this view that the presence of reduced sulfur is essential for initiating TSR reactions, and showed that the rate of TSR is directly proportional to the amount of reduced sulfur present in the system (Goldhaber and Orr, 1995; Machel, 2001; Cross et al., 2004; Zhang et al., 2008 and references therein). After temperature, the *p*H of the aqueous solution is probably the next most important factor controlling TSR reactions (Zhang et al., 2012). The dependence of the extent of TSR on *p*H conditions has been previously noted, with several laboratory studies of TSR having used highly acidic conditions to promote sulfate reduction (Kiyosu and Krouse, 1990; Goldhaber and Orr, 1995). At low *p*H conditions aqueous sulfate predominantly occurs as bisulfate (HSO_4^-), and quantum chemistry molecular modeling calculations have shown that bisulfate ions are much more reactive than stable aqueous sulfate ions (SO_4^{2-}) (Ma et al., 2008). The decades-held belief that TSR initiation requires the presence of reduced sulfur was disproven by a series of TSR simulation experiments using aqueous sulfate solutions ($CaSO_4$) buffered to *p*H conditions <4 (Zhang et al., 2012). It was further proposed that in natural environments where *p*H conditions are likely to be buffered to values >4, TSR reactions predominantly involve [$MgSO_4$] contact ion pair (CIP) rather than SO_4^{2-} or HSO_4^- (Ma et al., 2008; Zhang et al., 2012). While reduced sulfur species are not required to initiate the TSR reaction, the presence of H_2S does enhance the rate of TSR (Zhang et al., 2008). Consequently, a two-stage reaction scheme was proposed to explain this situation. This model postulates that initial sulfate reduction is slow and non-autocatalytic until a threshold concentration of H_2S is reached, at which point a faster H_2S-catalyzed sulfate reduction reaction becomes dominant (Zhang et al., 2008, 2012). It was suggested that H_2S reacts with hydrocarbons to form labile organic sulfur compounds (e.g., thiols, sulfides, polysulfides, etc.) that in turn catalyze TSR (Amrani et al., 2008; Zhang et al., 2008). In addition to the importance of intermediate oxidation-state sulfur species in the catalyzed TSR reaction, Xia et al. (2014) noted the significant role that intermediate oxidized organic compounds (e.g., organic acids, ketones, alcohols, etc.) play at this stage. Further, these authors proposed that once all of the C_{2+} hydrocarbons have been oxidized, the intermediate oxidized organic compounds are no longer available to participate in the catalytic sulfate reduction reaction, and a slow, non-autocatalytic, third stage of TSR commences (Xia et al., 2014). In spite of the substantial progress that has been made in understanding the details of the TSR reaction mechanism, significant knowledge gaps still exist.

Studies of the stable sulfur isotopic systematics of TSR in oil reservoirs have shown that TSR-generated H_2S typically has $\delta^{34}S$ values close to those of the source sulfate (gypsum or anhydrite) (Krouse, 1977; Worden and Smalley, 1996; Cai et al., 2003). However, theoretical models predict a substantial kinetic isotope effect associated with initial cleavage of the S–O bond of sulfate (Harrison and Thode, 1957; Goldstein and Aizenshtat, 1994). Laboratory experiments show that the S-isotopic fractionation between SO_4^{2-} and H_2S can be greater than 10‰ (Kiyosu, 1980; Kiyosu and Krouse, 1993) and at lower temperatures under open-system conditions can reach ~21‰ (Kiyosu, 1980; Watanabe et al., 2009; Oduro et al., 2011). A possible reason for the apparent contradiction between laboratory and field observations may be that the TSR reaction in oil reservoirs is rate-limited by the dissolution of solid sulfate minerals (Powell and Macqueen, 1984; Machel et al., 1995). In this scenario, aqueous sulfate is reduced faster than it can dissolve and diffuse to the site of reduction, producing ^{34}S-enriched H_2S with $\delta^{34}S$ values close to that of the solid sulfate source (Machel, 2001). Reactions of petroleum with TSR-derived H_2S have been proposed as a mechanism for producing organic sulfur compounds (OSCs) with ^{34}S-enriched values, distinct from the original $\delta^{34}S$ values of sedimentary organic sulfur (Orr, 1974; Powell and Macqueen, 1984; Hanin et al., 2002; Cai et al., 2003, 2009). This makes sulfur isotopes in petroleum potentially useful tracers for the occurrence and extent of TSR (Amrani, 2014).

Analysis of crude oil by gas chromatography (GC) and subsequent $^{34}S/^{32}S$ ratio measurements by multicollector inductively-coupled plasma mass spectrometry (MC-ICP-MS) enable analysis of individual S compounds (Amrani et al., 2009; Greenwood et al., 2014). Amrani et al. (2012) employed this technique to study a suite of oils from the Gulf of Mexico area (Jurassic Smackover Formation) and observed large variations in $\delta^{34}S$ (up to ~30‰) between alkylsulfides, alkylbenzothiophenes (BTs), and alkyldibenzothiophenes (DBTs) in a single oil. DBTs were often significantly depleted in ^{34}S compared with BTs. These $\delta^{34}S$ variations between DBTs and BTs were interpreted to reflect TSR-affected compounds (BTs) versus the original sedimentary organic sulfur represented by more thermally stable DBTs. More recently, a follow-up study of the Smackover Formation oils showed that thiaadamantanes (TAs), a presumed proxy for TSR (Wei et al., 2007), are also ^{34}S-enriched relative to DBTs, with $\delta^{34}S$ values close to those of the solid source sulfate (Gvirtzman et al., 2015). Similar ^{34}S-enriched values for TAs were also reported in oil samples from the Tarim Basin, China (Cai et al., 2016). Laboratory pyrolysis experiments involving $CaSO_4$ with distinct $\delta^{34}S$ values further support this interpretation (Amrani et al., 2012). These experiments also

showed a relatively large fractionation between OSCs and the parent sulfate.

The demonstrated utility of compound-specific sulfur isotope (CSSI) analysis for identifying reactive classes of compounds involved in TSR indicates that this technique has potential for providing additional information related to the TSR reaction network. In the present study, we attempt to further constrain details of the TSR reaction mechanism(s) by observing S-isotope fractionations among aqueous sulfate, H_2S, BTs, and DBTs during controlled TSR reactions. A series of laboratory pyrolysis experiments were performed involving *n*-hexadecane as an organic model compound representing petroleum, and two inorganic sulfur species ($CaSO_4$ and Na_2SO_4) with distinct $\delta^{34}S$ values. Compound-specific and bulk sulfur isotope methods were then applied to the products to determine the sulfur isotopic fractionations associated with specific organic and inorganic S compounds. The results provide insights into the overall TSR process that can be used to refine existing models of TSR reaction kinetics and geochemical proxies for determining the extent of TSR reaction.

2. EXPERIMENTAL

2.1. Reagents and standards

Solvents used in this study (CH_2Cl_2, hexane, etc.), purchased from BioLab (Jerusalem, Israel), were analytical grade and distilled before use. Sulfur hexafluoride (SF_6, 500 ppm in He) was purchased from Praxair (PA, USA). The sulfur isotope reference materials NBS-127 ($BaSO_4$; $\delta^{34}S = 21.1‰$), IAEA-S-1 (Ag_2S; −0.3‰), and IAEA-SO-6 ($BaSO_4$; −34.1‰) were purchased from the National Institute of Standards and Technology (NIST) and used for calibration of in-house standards. All other chemicals were purchased from Sigma–Aldrich (St. Louis, MO) and are analytical grade (>97% purity).

2.2. Pyrolysis experiments

The TSR experiments were conducted in sealed gold tubes with an internal diameter of 4.6 or 7.6 mm, wall thicknesses of 0.2 mm, and lengths of either ~25 or 70 mm, giving approximate reactor volumes of 1.0 mL. Mg^{2+} plus talc and silica was used as a mineral buffer at elevated temperatures to keep the in situ *p*H in a narrow range (*p*H ~ 3, Zhang et al., 2008). The approach used to regulate in situ chemical conditions in this study relies on chemical reactions that are known to proceed rapidly at the temperature and pressure conditions of the experiments (Saccocia and Seyfried, 1990; Seewald et al., 2000). Additional details regarding the mineral buffer approach are given by Zhang et al. (2008).

Each gold tube was loaded with 30 mg of talc, 30 mg of silica, and 450 mg of a distilled water solution containing 5.6 wt% $MgCl_2$, 10 wt% NaCl, and 0.56 wt% $CaSO_4$ or Na_2SO_4 depending on the form of solid sulfate used in the experiment. Five mg of hexadecane (n-C_{16}) was added as the organic reagent. Sulfate was added as $CaSO_4 * 2H_2O$, 10 mg or 126 mg, to a total sulfate (solid and solution) of 0.093 ± 0.001 mmol and 0.77 ± 0.02 mmol respectively, or as Na_2SO_4 (106 mg, or 0.77 ± 0.02 mmol total sulfate) depending on the particular experiment. Control experiments contained no sulfate (Table 1).

One end of each tube was crimped and sealed using an argon arc welder. Prior to loading the samples, the open-ended tubes were heated to 600 °C (exposed to air) to remove any residual organic material. After loading the reagents into the gold tubes, the tubes were flushed with Ar for 3 min to remove air. The open end of the tube was crimped and welded. Individual sealed gold tubes were subsequently placed in separate stainless-steel autoclaves and inserted into a pyrolysis oven. Pyrolysis experiments were conducted under isothermal conditions at a temperature of 360 °C and ranging from 10 to 180 h. Temperature was controlled to within 1 °C of the set point, and was monitored using a pair of thermocouples (one secured to the outer wall of each autoclave and a second one placed inside). Constant hydrostatic confining pressure was maintained at approximately 24.1 MPa (3500 psi) by a water pump to prevent rupturing of the gold tubes at elevated temperatures and to eliminate possible variations in the reactions as a function of pressure. When the desired reaction time was reached, the stainless-steel autoclave was rapidly cooled to room temperature by an automated cooling system. Once the autoclaves were depressurized, the gold tubes could be recovered for detailed analysis of their contents.

2.2.1. Recovery of samples after pyrolysis

To remove any potential organic contaminants from the exterior of the gold tubes, they were submerged in dichloromethane (DCM) for a minimum of 5 min and then rinsed with an additional aliquot of DCM and allowed to air dry. Following this cleaning procedure, the tubes were scored in three places and then frozen in liquid nitrogen for 5 min. Upon removal from the liquid nitrogen, the welded ends of each of the tubes were cut off and the body of each tube then cut into four equal pieces along the pre-scored lines. The four pieces of the tube were quickly placed into a 20 mL screw-cap vial with a Teflon® lined cap containing 5 mL of DCM and allowed to soak overnight (12–20 h). The vials containing the gold tube pieces were then sonicated for approximately 1 h, and then placed into an ice bath for a minimum of 1 h to minimize loss of volatile components. The vials were then opened for a minimal amount of time to allow for the removal of the pieces of gold tubing and their transfer to a second 20 mL screw-cap vial with a Teflon® lined cap containing 5 mL of DCM. The gold pieces in this second vial were treated in the same manner as the first vial (i.e., soaked overnight, sonicated 1 h, ice bath 1 h). Subsequently, the second vial was opened and each piece of gold tubing was removed, cut open lengthwise, and rinsed with additional DCM to remove all solid residues from the gold. The rinse solvent and solid residues were collected with the 5 mL of solvent in the second vial, which was then combined with the contents of the first vial.

Table 1
Quantities of the reagents used for the gold-tube pyrolysis experiments.

	Pyrolysis time (h)	C_{16} (mg)	C_{16} (mmol)	Talc (mg)	Silica (mg)	Solution[a] (mg)	Sulfur (solid)[b] (mmol)	Sulfur in solution[c] (mmol)	Total S[d] (mmol)
Limited $CaSO_4$	10–180	5.0	0.022	30	30	450	0.075	0.018	0.093
Excess $CaSO_4$	10–180	5.0	0.022	30	30	450	0.75	0.018	0.77
Na_2SO_4	10–180	5.0	0.022	30	30	450	0.75	0.018	0.77
Na_2SO_3	10–180	5.0	0.022	30	30	450	0.069	0	0.069
Elemental S	10–89	5.0	0.022	30	30	450	0.10	0	0.10

[a] Mineral buffer water solution containing 5.6 wt% $MgCl_2$ and 10 wt% NaCl. When sulfate was the sulfur source, 0.56 wt% Na_2SO_4 or $CaSO_4$ was also added to the solution.
[b] Sulfur source added to the gold tube as a solid ($CaSO_4$, Na_2SO_4, Na_2SO_3 and elemental S).
[c] Soluble sulfate concentration in the mineral buffer solution added to the gold tube.
[d] Sum of soluble and solid sulfur in each tube.

2.3. GC–MS and GC-FPD analysis

A GC coupled to a Quadrupole mass spectrometer (GC/MS Agilent 7890/5750) was used to identify individual OSCs. About 1 µl of sample was injected into the GC at a split ratio of 10:1 and a constant temperature of 320 °C. Helium was used as the carrier gas at a constant flow rate of 1.5 ml/min. We used two oven temperature programs: (1) 60 °C for 5 min, 60–320 °C at 10 °C/min, and 320 °C for 10 min for a direct comparison with GC-MC-ICPMS and GC coupled to flame photometric detector (FPD) conditions; and (2) 50 °C for 5 min and then heated in a rate of 5 °C min^{-1} up to 320 °C where it was held for 20 min for the GC–MS. Both GC–MS and GC-FPD were equipped with a DB5-MS capillary column 30 m in length, 0.25 mm in diameter, and with a 0.25 µm film thickness (Agilent). The MS source was operated at 300 °C in electron impact mode at 70 eV.

Peaks of specific compounds (BT, DBT, 2-Phenylthiophene, Thiophenol, etc.) were identified against the retention times and MS spectra of authentic standards. Quantification of the gold tube products was made using an internal standard method by adding 100–250 µl of squalane standard solution (10 pmol $µl^{-1}$ or 20 pmol $µl^{-1}$) to each sample prior to the evaporation and concentration of the samples by a gentle stream of N_2. Relative response factors (RRF) of each compound against the squalane were calculated using calibration curves in the range of 1–50 pmol $µL^{-1}$. Precision of the quantification was estimated by performing duplicate analyses of a few samples to represent the entire sample set. The standard deviation of the duplicates is in the range of 0.2 to 4.4 nmol (RSD 4 to 26%) depends on the sample concentration.

2.4. GC-MC-ICP-MS analysis of $\delta^{34}S$ of specific compounds

2.4.1. Instrumental set-up

The compound-specific S-isotope analyses were conducted with a GC coupled to a multi-collector inductively coupled plasma mass spectrometer (GC-MC-ICPMS) based on the system reported by Amrani et al. (2009). We used two different GC-ICP-MS systems in this study. The first, housed in the Division of Geological and Planetary Sciences at the California Institute of Technology, consists of an Agilent 6890 GC that is coupled to a Thermo Scientific Neptune multi-collector (MC) ICP-MS via a heated transfer line (Amrani et al., 2009, 2012). The second, operated by the Earth Sciences Institute at the Hebrew University of Jerusalem Israel, consists of a Clarus 580 GC (Perkin Elmer) or Trace GC (Thermo Fischer), equipped with a Agilent DB5-MS, 30 m, 0.25 mm, 0.25 µm thickness capillary column and coupled to a Thermo Scientific Neptune *plus* MC-ICP-MS (Said-Ahmad and Amrani, 2013; Gvirtzman et al., 2015). One µl of sample solution was injected to the inlet at a constant temperature of 320 °C. Helium was used as carrier gas at a constant flow rate of 1.5 mL/min. The oven temperature program of the GC was: 60 °C for 5 min, 60 to 320 °C at 10 °C/min, and maintained at 320 °C for 20 min. Both GC-MC-ICPMS systems showed similar performance and similar results (Said-Ahmad and Amrani, 2013; Gvirtzman et al., 2015). SF_6 gas (in helium) was used for calibration and injected at the beginning and end of each sample analysis. The SF_6 ($+2.8 \pm 0.5‰$ or $-1.9 \pm 0.5‰$) was calibrated against an in–house standard mixture that consisted of: 2-methyl BT (+14.4‰), 2-adamantane thiol (+17.4‰), DBT (+12.9‰ or +3.3‰), octyl sulfide (−0.4) and 4,6, dimethyl DBT (−8.7). These in-house standards were individually calibrated against IAEA standards (see Section 2.1) EA-IRMS and/or by MC-ICPMS as detailed in Amrani et al. (2009) and Said-Ahmad and Amrani (2013) and Gvirtzman et al. (2015). Calibration of the SF_6 against the in–house standard mixture was done every 3–5 samples.

Results of isotopic analyses are expressed in conventional $\delta^{34}S$ notation as per mil (‰) deviations in the $^{34}S/^{32}S$ ratio from the Vienna Canyon Diablo Troilite (VCDT) standard:

$$\delta^{34}S = ({}^{34}R_{sample}/{}^{34}R_{std}) - 1 \quad (1)$$

where, ^{34}R is the integrated $^{34}S/^{32}S$ ion-current ratio of the sample and standard peaks. Data processing employed algorithms that are implemented in Visual Basic code

within Microsoft Excel (Ricci et al., 1994; Sessions et al., 2001). Ion currents were integrated by the Neptune software (v. 3.1.0.27) in 189 ms increments and exported to Excel in ASCII format. Further details about the peak integration, calibration and processing are provided in Amrani et al. (2009) and Amrani et al. (2012). Precision and accuracy of standards were better than 1‰ (1σ).

2.5. Sulfate and hydrogen sulfide quantification and S-isotope analysis

2.5.1. Quantification

For each experiment conducted in the gold tubes, a duplicate was run in parallel to collect the residual sulfate and H_2S. H_2S from the gold tube was bubbled through a 5 wt% $AgNO_3$ solution and precipitated as solid Ag_2S. The solid was cleaned using distilled water in order to remove any nitrate, washed with acetone, dried and weighed. In several cases, H_2S was also quantified using a GC (Agilent 7890A), equipped with a flame ionization detector (FID) and two thermal conductivity detectors (TCDs). H_2S was measured by TCD after the gold tube was pierced in an evacuated glass device via the GC gas sampling loop. The oven temperature for the hydrocarbon gas analysis was initially held at 50 °C for 3 min, ramped from 70 °C to 180 °C at 25 °C/min, and then held at 180 °C for 5 min, where it was held at 90 °C for the inorganic gas analysis. This device was calibrated before the gold tube gas analysis by analyzing a standard gas mixture. The composition of the standard gas was: methane (5%), ethane (3%), propane (1%), CO_2 (5%), and H_2S (5%), balanced with N_2. The reproducibility of this method was within 10% (RSD).

The residual sulfate was washed from the gold tube into a 20 mL glass vial. An aqueous solution of 5 wt% $BaCl_2$ was added in excess to the glass vial and then heated to 70 °C overnight. The solution was filtered through a Buchner funnel using 47 mm filter (Whatman©) and the white precipitate was washed with distilled water and weighed. The analytical error for this method was estimated at 0.005 mmol to 0.01 mmol. In some cases the residual sulfate was also quantified using ion chromatography (IC) for comparison. The samples were filtered through a syringe filter (nominal pore size 0.20 μm) and injected into the IC with no further purification. The analytical error of the IC quantification was estimated to be 0.03 mmol (4.1% relative), based on the difference between the measured and known concentration of a standard sample.

2.5.2. Bulk sulfur isotope analysis

The $\delta^{34}S$ values of both inorganic sulfide and sulfate were measured using an Elemental Analyzer (Flash 1112 series) connected through a Conflow III interface to an Isotope Ratio Mass Spectrometer (IRMS) (Delta Plus, ThermoFisherScientific). The sulfur isotope reference materials (see Section 2.1) were used for calibration of in-house organic and inorganic standards and Ag_2S and $BaSO_4$ samples from the pyrolysis experiments. The precision of the measurement of standards were better than 0.3‰.

3. RESULTS

3.1. TSR simulation experiments

Three sets of experiments were performed representing the following experimental conditions as detailed in Table 1: (1) experiments with a limited amount of $CaSO_4$ and excess hydrocarbon to simulate a closed system for sulfate, (2) experiments with an excess amount of $CaSO_4$ and limited hydrocarbon to simulate an open system for sulfate, and (3) experiments with an excess amount of Na_2SO_4 as the sulfate source rather than $CaSO_4$ to study the effect of dissolution rate on S-isotopic fractionation during TSR.

3.1.1. Limited $CaSO_4$ experiments

These experiments were performed with a limited amount of $CaSO_4$ (0.093 mmol) for periods of time ranging from 10 to 180 h at 360 °C (Table 1). Fig. 1a clearly shows the reduction of sulfate and formation of H_2S. Sulfate was almost completely consumed during the course of the reaction under these conditions.

At early TSR stages, the amounts of BT and DBT produced were small (0–4 nmol of BT and 0–0.2 nmol of DBT), but after 20 h significant amounts of BT, DBT, and H_2S production were observed. The amount of DBT after 40 h remained relatively constant (~10 nmol), while BT reached a maximum amount of about 30 nmol after 89 h and then started to degrade (Fig. 1b).

Experiments were conducted with initial $CaSO_4$ reactant of three distinct $\delta^{34}S$ values (+12.8‰, +2.4‰ and −5.3‰) to follow the S-isotope fractionation of OSC with more confidence (Table 2). Another experiment was performed to measure the residual sulfate fractionations and concentrations (initial $\delta^{34}S = 19.6$‰). The results are presented as the difference between the $\delta^{34}S$ values of reactant sulfate and product according to the following equation:

$$\Delta^{34}S = \delta^{34}S_{product} - \delta^{34}S_{intial\ sulfate} \quad (2)$$

The results of these three experiments were in good agreement (Table 2), and Fig. 1c presents the average $\delta^{34}S$ data from all three experiments. We chose to focus on BT and DBT as representative of OSCs produced via TSR because of their relatively high abundance, differential thermal stability, and ease of chromatographic separation (Fig. 2), the latter of which allowed for more reliable $\delta^{34}S$ measurements.

The $\delta^{34}S$ value of sulfate was almost constant during the course of the reaction and did not change significantly (0.5‰) relative to the initial sulfate. The $\delta^{34}S$ value of the newly formed H_2S was initially (20 h) 7.1‰ lower than that of initial sulfate, and then rapidly converged to the $\delta^{34}S$ of initial sulfate (Fig. 1c).

Large S-isotopic differences between the initial sulfate and the OSCs in the early stages of the TSR experiments were consistently observed in all three experiments (Fig. 1c). A fractionation of 18.8‰ was observed between BT and the initial sulfate during the first 10 h (Fig. 1c). After 20 h BT and DBT had similar $\delta^{34}S$ values, about 10.6‰ lower than the initial sulfate, while H_2S at this time was depleted in ^{34}S by about 7.1‰. This isotopic difference

gradually decreased as the pyrolysis time progressed, with H_2S being the fastest to approach the $\delta^{34}S$ of the source sulfate, while BT and DBT changed at slower rates. BT was consistently ^{34}S-enriched relative to DBT (3 to 5‰) and never reached the $\delta^{34}S$ of the H_2S and sulfate, but was about 2‰ ^{34}S-depleted.

3.1.2. Excess $CaSO_4$ experiments

In these experiments, the $CaSO_4$ (0.77 mmol) was in large excess, 8-fold, relative to the "limited" $CaSO_4$ experiments. Consequently only about 16% of the $CaSO_4$ was consumed after 180 h (Fig. 3a), while in the "limited" experiments almost all the $CaSO_4$ was consumed.

Significant amounts of H_2S, BT, and DBT were observed only after 40 h of reaction (Fig. 3b). The amounts of BT and DBT were higher than those of the limited experiments by 2- and 15-fold, respectively. BT was produced faster than DBT and at 40 h reached its maximum concentration, while DBT reached its maximum production at 180 h. Unlike the limited sulfate experiments, the amount of BT decreased significantly at later TSR stages. In this set of experiments, we also clearly identified another representative compound, 2-phenylthiophene (PT) that has a lower thermal stability than BT (Fig. 2). This compound (PT) can aid our understanding of the system because the lower thermal stability leads to more instantaneous reactions with H_2S, which is then reflected in its $\delta^{34}S$ value. PT's production was significant only after 40 h, and its concentration was much lower than BT and DBT reaching a maximum of 14.2 nmol after 89 h.

Experiments with two different initial $CaSO_4$ $\delta^{34}S$ values (12.8‰ and 2.4‰) were conducted in order to check the reproducibility of the results. Another experiment was performed to measure the residual sulfate fractionations and concentrations (initial $\delta^{34}S = 19.6$‰). The reported results are the average fractionation values of these two experiments from initial sulfate (Fig. 3c; Table 2). No significant S-isotopic fractionation was observed between sulfate and H_2S throughout all stages of the reaction, and they both had $\delta^{34}S$ values similar to the initial $CaSO_4$. BT and DBT showed similar trends relative to the limited-$CaSO_4$ experiments, but in this case the S-isotopic values of BT did not reach a plateau even at the latest reaction time. The initial $\delta^{34}S$ values of BT and DBT were lower than in the limited-$CaSO_4$ experiment. PT experienced a more rapid S-isotopic convergence to the initial sulfate value than either the BT or DBT. Its value became heavier than BT or DBT and reached the initial sulfate value after 180 h.

3.1.3. Experiments with excess Na_2SO_4

These experiments were conducted in order to simulate TSR with an excess of the fully soluble Na_2SO_4 (0.77 mmol) to study the effect of sulfate dissolution rate on S-isotopic fractionation. Two distinct Na_2SO_4 reagents with initial $\delta^{34}S$ values of −5.3‰ and +1.0‰ were chosen for these experiments in order to verify the reproducibility of the results (Table 3). Compared to the excess-$CaSO_4$ experiments, the consumption of Na_2SO_4 was similar, although a bit higher (about 0.09 mmol) and the H_2S yields were similar (Fig. 4a).

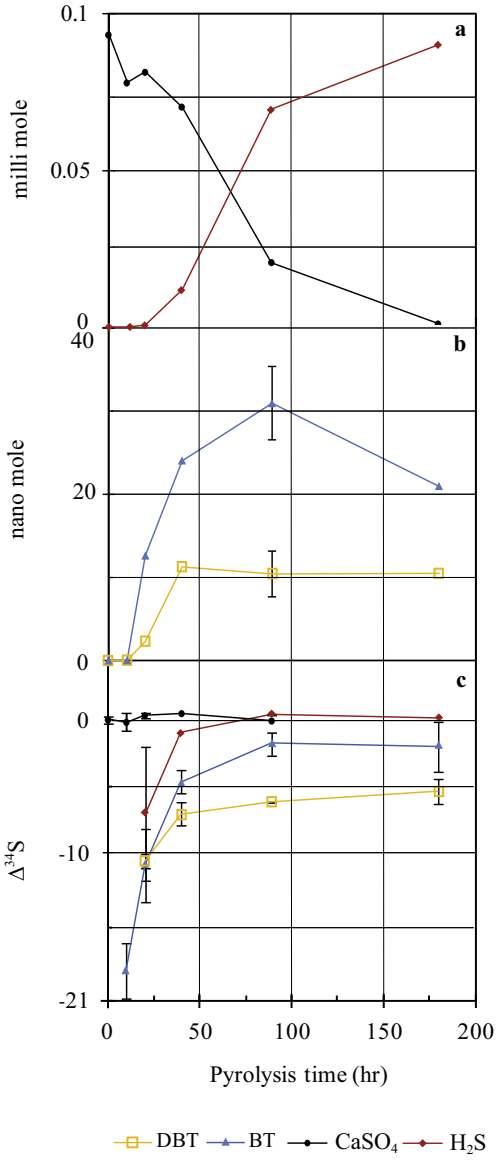

Fig. 1. Results from TSR simulation reactions with limited amount of $CaSO_4$ (0.093 mmol). (a) The consumption of sulfate versus the formation of H_2S. (b) OSC concentration (nmol) as a function of pyrolysis time. (c) Isotopic fractionation of BT, DBT, H_2S and residual sulfate normalized to initial $\delta^{34}S$ of sulfate, plotted against pyrolysis time. Each data point represents the average fractionation ($\Delta^{34}S$) from supplied sulfate of three different experiments with different $\delta^{34}S$ of initial sulfate (12.8‰, 2.4‰ and −5.3‰). The error bars represent 1σ standard deviation of these experiments ($n = 2$ or 3).

Significant formation of OSCs began after 20 h (Fig. 4b). BT and PT reached their maximum concentrations after 40 h (60 and 75 nmol, respectively) while DBT reached its maximum concentration of 355 nmol after 89 h. These maximum OSC concentrations were significantly higher than those observed for the $CaSO_4$ experiments. However, the thermal degradation of OSCs was also very intensive, and after 180 h only DBT, the most thermally stable compound of the three, remained in the

Table 2
$\delta^{34}S$ values for the individual gold-tube pyrolysis experiments with distinct $CaSO_4$ reagents.

	Initial calcium sulfate ($CaSO_4$) = −5.3‰			Initial calcium sulfate ($CaSO_4$) = 2.4‰			Initial calcium sulfate ($CaSO_4$) = 12.8‰		Initial calcium sulfate ($CaSO_4$) = 19.6‰		$\Delta^{34}S = \delta^{34}S$(product) − $\delta^{34}S$(initial sulfate)				
	Pyrolysis time (h)	BT (‰)	DBT (‰)	BT (‰)	DBT (‰)	2-PT (‰)	BT (‰)	DBT (‰)	H_2S (‰)	Residual sulfate (‰)	$\Delta^{34}S$ BT (‰)	$\Delta^{34}S$ DBT (‰)	$\Delta^{34}S$ 2-PT (‰)	$\Delta^{34}S$ H_2S (‰)	$\Delta^{34}S$ residual sulfate(‰)
Limited $CaSO_4$	10	−22.6	–	–	–	–	−7.4	–	–	19.4	–18.8 ± 2.1	–	–	–	−0.2
	20	−15.2	−16.2	−11.5	–	–	4.1	2.6	2.2[a]	19.9	–10.8 ± 2.7	–10.6±0.5	–	−7.1 ± 5.0[a]	0.3
	40	−9.0	−12.6	−2.9	–3.7	–	7.8	5.0	11.9	20.1	–4.7±0.9	−7.1±0.9	–	−0.9	0.5
	89	−6.5	−11.4	–	–	–	10.4	6.7	13.2	19.5	–1.8±0.8	−6.1±.0	–	0.4	−0.1
	180	−5.6	−11.5	−1.6	–3.1	–	10.9	8.5	13.0	–	–2.1±1.9	−5.3±1.0	–	0.1	n.d
Excess $CaSO_4$	10	–	–	–	–	–	–	–	–	19.5	–	–	–	–	−0.1
	20	–	–	−12.7	–	–	–	−0.9	12.9	19.2	−15.1	−13.7	–	0.1	−0.4
	40	–	–	−6.4	–8.5	−2.2	2.9	2.0	12.5	19.3	–9.4±0.8	–10.9±0.1	−4.6	−0.3	−0.3
	89	–	–	−1.0	–5.9	3.1	5.3	3.6	12.3	20.2	–5.5±2.9	−8.3±0.6	0.7	−0.5	0.6
	180	–	–	−1.2	–6.2	1.2	8.2	4.6	12.6	19.8	–4.1±0.7	−8.6±0.3	−1.2	−0.2	0.2

'–' Could not be detected or not measured.
[a] Another measurement of −3.5‰ for H_2S was taken from initial $CaSO_4$ of 2.4‰.

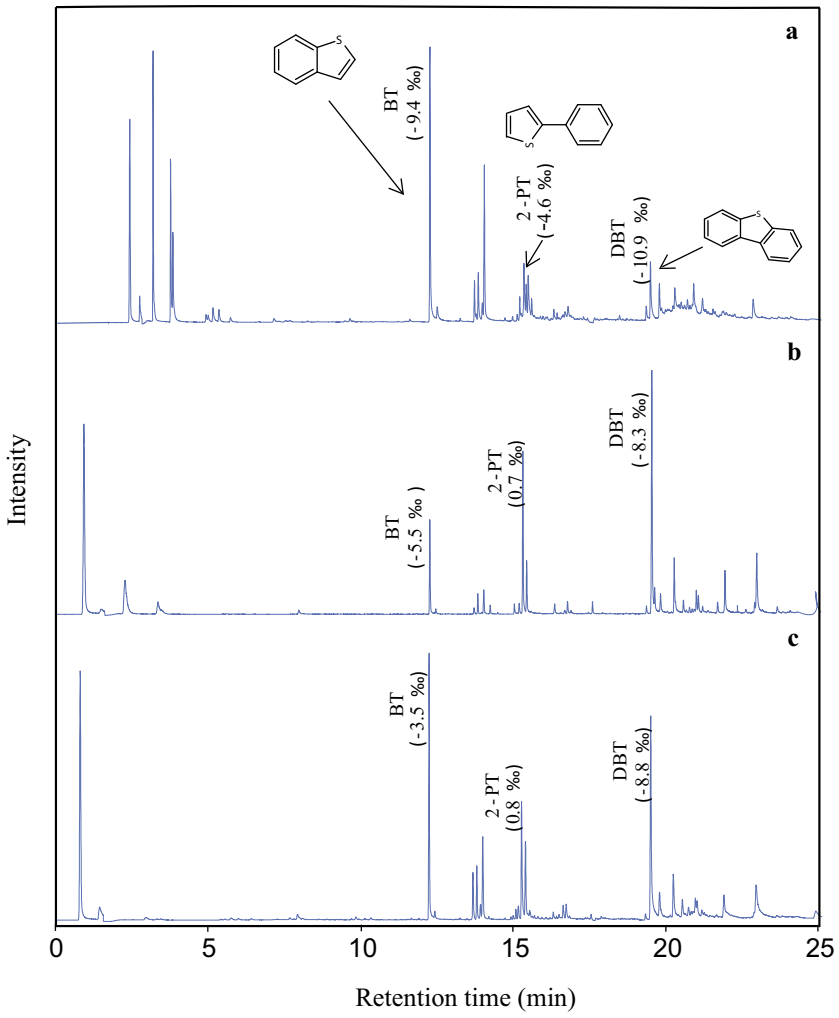

Fig. 2. GC-ICPMS chromatograms of three successive experiments with excess-$CaSO_4$ (0.77 mmol) (a) 40 h (b) 89 h. (c) 180 h. BT, PT and DBT are marked with their isotopic fractionation relative to the initial sulfate source.

system. The initial S-isotopic fractionation of H_2S from the initial sulfate, which could be measured after 20 h, was 12.4‰, and after 89 h it had increased to about 14‰. The remaining sulfate became gradually ^{34}S-enriched up to 3.9‰ relative to the initial sulfate after 180 h. In contrast, the experiments with $CaSO_4$ did not change the $\delta^{34}S$ values of the sulfate during the reaction (Figs. 1 and 3).

The S-isotopic fractionation for OSCs at the early stages was the largest observed of all TSR experiments (Fig. 4c) and reached 22.2‰ for BT after 10 h. PT and DBT were measured after 20 h and their fractionation relative to the initial sulfate was 17.5‰ and 18.0‰, respectively. Unlike the experiments with $CaSO_4$, OSCs did not converge on the $\delta^{34}S$ values of sulfate as the reaction progressed beyond 20 h. BT did become ^{34}S-enriched for reaction times between 10 and 20 h, but did not change much at 40 h, and later it was completely degraded and disappeared from the system. DBTs fractionation relative to the initial sulfate started at 17‰, increased to 20.2‰, and then returned to 17‰ to the end of the reaction.

The intensity of the reaction of Na_2SO_4 relative to that of $CaSO_4$ is evident in Fig. 5. In the Na_2SO_4 experiments (Fig. 5c), n-C_{16} and its breakdown products (n-C_{14} to n-C_9) were completely consumed by the longest experimental time (180 h), thus limiting the TSR reaction and the formation of additional H_2S (Fig. 5). Fused-ring aromatic compounds (e.g., naphthalene) become a dominant hydrocarbon with increased reaction time under all of the experimental conditions studied. The concentrations of these aromatic compounds increases from the limited-$CaSO_4$ experiment (Fig. 5a) to the most reactive Na_2SO_4 conditions (Fig. 5c) with the excess-$CaSO_4$ experiment in between (Fig. 5b), reflecting the intensity of the TSR reaction. A similar order can be seen for the increased formation of elemental S among the different sets of experiments probably because of the decreasing amounts of hydrocarbons available to reduce it to H_2S.

3.2. Non-TSR Pyrolysis experiments

In order to better understand the TSR mechanism, we also studied secondary reactions of TSR products (elemental S and SO_3^{-2}) with n-C_{16}. The molar S quantities, time

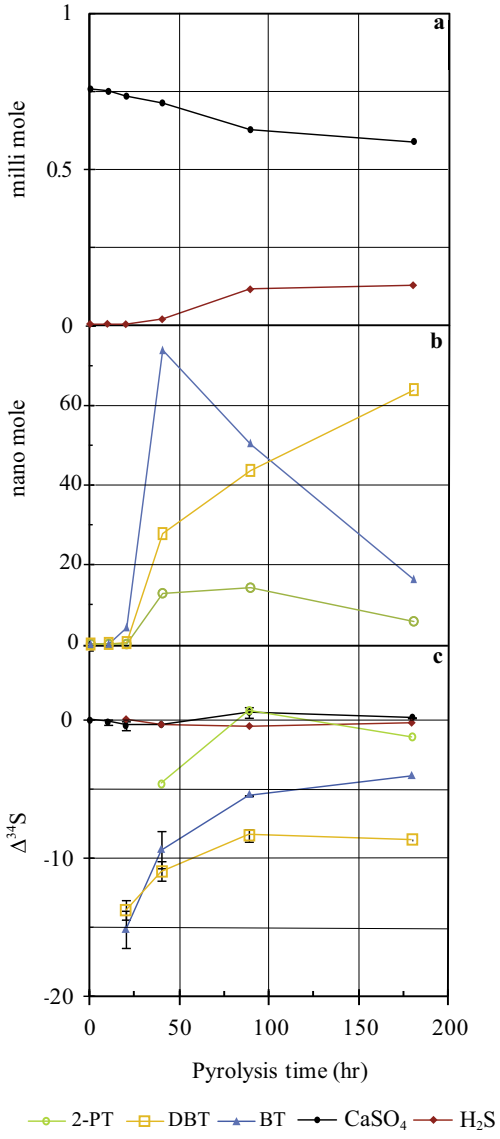

Fig. 3. Results of TSR simulation reactions with an excess of $CaSO_4$ (0.77 mmol). (a) The consumption of sulfate verses the formation of H_2S. (b) OSC concentration (nmol) against pyrolysis time. (c) Isotopic fractionation of BT, DBT, H_2S and residual sulfate normalized to initial $\delta^{34}S$ of sulfate, plotted against pyrolysis time. Each data point represents the average fractionation ($\Delta^{34}S$) from initial sulfate of three different experiments with different $\delta^{34}S$ values of initial sulfate (12.8‰, 2.4‰). The error bars represent the 1σ standard deviations of these experiments ($n = 2$).

intervals and temperature were similar to the limited-$CaSO_4$ experiments (see Section 2).

3.2.1. n-C_{16} pyrolysis experiments with elemental sulfur (S_8)

These experiments were conducted to determine the fractionation between reduced S species and OSCs. It is important to note that the reaction with elemental S and hydrocarbons is so intense at 360 °C that elemental S is rapidly converted to H_2S. Consequently, this experiment may actually represent the fractionation associated with the reaction of hydrocarbons with H_2S rather than elemental S. Measured values for this fractionation, when combined with the total fractionation for OSC formation via sulfate reduction, allows for the calculation of the net sulfur isotopic fractionation associated with the reduction of sulfate (or sulfite) to elemental S or H_2S using the OSCs $\delta^{34}S$ values.

In these experiments, elemental S (0.1 mmol) and *n*-C_{16} were reacted under identical experimental conditions as in the TSR experiments. The only sulfur source in these experiments was elemental S.

The results showed a rapid formation of BT and DBT (after 10 h), and a temporal pattern that was different from the TSR experiments (Fig. 6a). In the TSR experiments, DBT continuously increased in concentration with reaction time while BT was either constant (limited-sulfate experiment) or reduced (excess-sulfate experiments) with extent of reaction. In contrast to the elemental S experiments, DBT remained constant at about 10 nmole and BT increased up to about 70 nmol (Fig. 6a). The total concentrations of these compounds were in the range of the excess-sulfate TSR experiments. The fractionations of BT and DBT from the initial elemental S (+1.2‰) were 0.5 to 2.5‰, respectively (Table 4). BT was consistently ^{34}S-enriched relative to DBT by about 0.5–1.5‰, and there were no apparent effects of the reaction time on the fractionations.

3.2.2. n-C_{16} pyrolysis experiments with sodium sulfite (Na_2SO_3)

The rate-limiting step in TSR is thought to be the cleavage of the first S-O bond in sulfate leading to the formation of sulfite from sulfate (Goldstein and Aizenshtat, 1994; Ma et al., 2008). These experiments were conducted in order to measure the isotopic fractionation related to the reaction of sulfite with organic matter (Table 5). The results of these experiments are presented in Fig. 6. Significant fractionation between BT and DBT and initial sulfite were observed over the course of the reaction, up to 9.0‰ for DBT (Fig. 6b). However, no fractionation between H_2S and the original sulfite was measured, contrary to the observations from the limited-sulfate experiments.

4. DISCUSSION

4.1. Isotope fractionation during TSR

4.1.1. Kinetic isotope fractionation

Results of the present study support the two-stage model that was suggested in earlier work by Zhang et al. (2008). Fig. 7 illustrates these two stages and their associated chemical reactions, based on the S-isotopic patterns of individual OSCs observed in the present study. The first reaction in the initial stage of TSR involves cleavage of an S–O bond in the aqueous sulfate ion (Eq. (3); Ma et al., 2008), which is accompanied by a large kinetic isotopic effect (Harrison and Thode, 1957; Goldstein and Aizenshtat, 1994).

$$HSO_4^- + C_xH_y \longrightarrow HSO_3^- + C_xH_{y-2} + H_2O \quad (3)$$

Table 3
$\delta^{34}S$ values for the individual gold-tube pyrolysis experiments with Na_2SO_4.

		Sodium sulfate (Na_2SO_4) = 1‰				Sodium sulfate (Na_2SO_4) = −5.3‰		$\Delta^{34}S = \delta^{34}S$(product) − $\delta^{34}S$(initial sulfate)				
	Pyrolysis time (h)	BT (‰)	DBT (‰)	2-PT (‰)	H_2S (‰)	Residual sulfate (‰)	BT (‰)	DBT (‰)	$\Delta^{34}S$ BT (‰)	$\Delta^{34}S$ DBT (‰)	$\Delta^{34}S$ 2-PT (‰)	$\Delta^{34}S$ H_2S (‰)	$\Delta^{34}S$ residual sulfate (‰)
Na_2SO_4	10	–	–	–	–	0.8	−27.5	–	−22.2	–	–	–	−0.3
	20	−18.1	−17.8	−16.5	−11.4	2.0	−20.4	−22.4	−17.1 ± 2.8	−18.0 ± 1.2	−17.5	−12.4	1.0
	40	−16.6	−19.2	−14.2	−9.3	3.6	–	–	−17.6	−20.2	−15.2	−10.3	2.6
	89	–	−16.2	–	−12.9	4.1	–	–	–	−17.2	–	−13.9	3.1
	180	–	−16.3	–	−13.5	4.9	–	–	–	−17.3	–	−14.5	3.9

'–' Could not be detected or not measured.

Harrison and Thode (1957) empirically determined a fractionation factor of about 22‰ for the chemical reduction of sulfate to H_2S over a temperature range of 18–50 °C. These authors suggested that the rate-limiting step is the SO_4^{2-} to SO_3^{2-} reduction and support this with theoretical calculations. Grinenko et al. (1969) performed TSR experiments at the range of 100 to 290 °C and reported fractionations of 18.7‰ to 8.6‰, respectively with a clear temperature dependence. Both Grinenko et al. (1969) and Harrison and Thode (1957) studies used highly acidic and reducing reagents (e.g., HI, H_3PO_2, and HCl) or H_2, but no hydrocarbons in their experiments. More recent laboratory experiments demonstrated fractionations of up to 20.8‰ at 150–200 °C and under open-system conditions, using amino acids as the reductant (Watanabe et al., 2009). Oduro et al. (2011) conducted both closed-system pyrolysis (175–298 °C in Carius tubes) and open-system pyrolysis (258 °C and 298 °C) experiments and demonstrated fractionations of up to ~15.6‰ and 19.2‰, respectively, using glycine as the carbon source. These previous studies are difficult to compare to our results because of the different reagents (amino acids, H_2 etc.), chemical conditions (e.g., *p*H), temperatures and type of pyrolysis (open or closed) used. Other TSR experiments, closer in their operating conditions to the present work, were conducted in a closed system over temperatures ranging from 250 to 340 °C, and reported maximum fractionations of 8 to 10‰ with no clear dependence on temperature (Kiyosu, 1980). Later work by Kiyosu and Krouse (1990) suggested that the kinetic isotopic effect (KIE) during TSR is a function of temperature:

$$10^3(\alpha - 1) = 3.32 * \frac{10^6}{T^2} - 4.19 \quad (4)$$

where, α is the fractionation factor for sulfate and T is the temperature in Kelvin. Using Eq. (4), α is calculated to be 1.0046 (at $T = 633$ K), which translates to 4.6‰ at our experimental temperature. According to these authors, this reduction in the fractionation relative to their early work by 4–5‰ (Kiyosu, 1980), was caused by the fact that in the later work H_2S was detected only after the entire pool of sulfate was consumed. They suggested that the reduced S was in another intermediate form before it was converted to H_2S (Kiyosu and Krouse, 1990). In the present study, both H_2S and sulfate were present in the system, and is therefore more comparable to the earlier work (Kiyosu, 1980) than the later study (Kiyosu and Krouse, 1990). The previously observed fractionation of 8–10‰ (Kiyosu, 1980) is closer to the values measured for sulfate-sulfide fractionation at the early stages of both the limited-$CaSO_4$ experiment (7.1‰) and the Na_2SO_4 (12.4‰) experiment, indicating that these initial fractionations are probably due to the kinetic isotopic effect.

4.1.2. Organosulfur species formation

Compared to the fractionations observed in the generated H_2S, significantly larger fractionations were recorded by the early formed BT in the limited-$CaSO_4$ and the Na_2SO_4 experiments, with magnitudes of 18.8‰ and 22.2‰, respectively (Figs. 1c and 4c). These values were

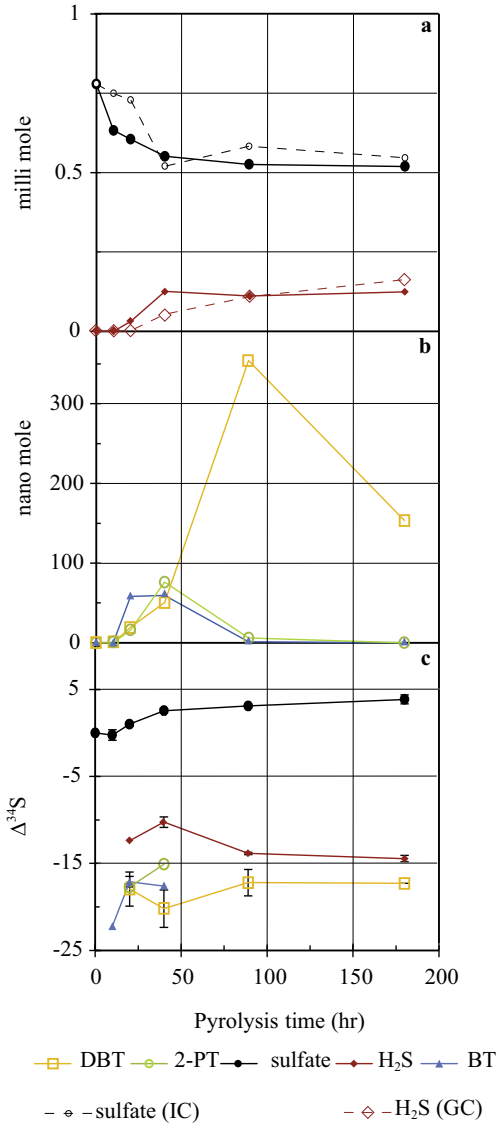

Fig. 4. Results of TSR simulation reactions with an excess amount of Na_2SO_4 (0.77 mmol). (a) Sulfate consumption and sulfide production (mmol compound) as measured gravimetrically, against pyrolysis time. H_2S (GC) – measured by GC-TCD system and Sulfate (IC) – measured by ion chromatograph. (b) OSC concentration (nmol) against pyrolysis time (c) isotopic fractionation of BT, DBT, H_2S and residual sulfate against pyrolysis time. Data points represent the average of two different experiments with different $\delta^{34}S$ of initial sulfate (+1.0‰ and −5.3‰). The error bars represent the 1σ standard deviations of these experiments ($n = 2$).

observed after 10 h of reaction when H_2S was yet to be detected. In contrast, pyrolysis experiments with n-C_{16} and elemental S form OSCs with only 1–3‰ ^{34}S depletion relative to their initial S source (Fig. 6a). The $\delta^{34}S$ values of BT and DBT were similar, but DBT was consistently about 1–2‰ depleted and the BT was closer to the source elemental S (Fig. 6a). A detailed discussion of the $\delta^{34}S$ values of OSCs formed during TSR reactions is provided in Section 4.2.

In similar gold-tube pyrolysis experiments (360 °C) with adamantane (a 10-carbon hydrocarbon with a cage-like structure) and elemental S, a ^{34}S depletion of 0.5–3.4‰ for the newly formed thiaadmantanes and BTs was observed (Gvirtzman et al., 2015). Previous experiments with different reduced S species ($H_2S_{(g)}$, elemental S, and $(NH_4)_2S_{(aq)}$) with 1-tetradecene at lower temperatures (200 °C) are in agreement with these results and show small fractionations (0.5 to 4‰) for OSC formation (mainly thiophenes, Amrani et al., 2006).

These experimental results indicate that there is only minor fractionation in the formation of OSCs from reduced S species such as H_2S and elemental S at high temperature. This fractionation (usually < 4‰) cannot explain the large S-isotope fractionation between source sulfate and OSC, up to ~22‰, in the initial stages of the present TSR experiments (Fig. 4c). If the $\delta^{34}S$ values observed in the OSCs represent the very early sulfate-H_2S fractionation (plus an additional 2–3‰ for the formation of OSC from H_2S), then a large disagreement exists between the current work and the earlier studies of Kiyosu (1980) and Kiyosu and Krouse (1990). Other mechanisms (in addition to the KIE) need to be investigated to assess their potential impact on observed S-isotope fractionations in TSR reactions.

4.1.3. Closed-system distillation

To determine if our isotopic data can be explained by closed-system distillation ("Rayleigh distillation"), the following equations can be used to predict fractionation between sulfate and H_2S as a function of the fractional extent of reaction (f) as determined by the consumption of sulfate:

$$\delta_{RS} = \delta_{initial} - \alpha \ln(1-f) \quad (5)$$

$$\delta_{ip} = \delta_{initial} - \alpha[1 + \ln(1-f)] \quad (6)$$

$$\delta_{AP} = \delta_{initial} + \alpha\left(\frac{1-f}{f}\right) * \ln(1-f) \quad (7)$$

where, δ_{RS} is the residual sulfate isotopic composition, $\delta_{initial}$ is the initial sulfate value, δ_{AP} is the accumulated product value (H_2S), δ_{ip} is the instantaneous product (H_2S) value, and α is the relevant fractionation factor. Calculations were made using two distinct fractionation factors (α). First, $\alpha = 1.011$ based on the measured H_2S fractionation relative to source sulfate at the earliest time that it could be detected (20 h) in the Na_2SO_4 experiment. Second, $\alpha = 1.020$ based on the BTs fractionation relative to source sulfate after 10 h (22.2‰) in the Na_2SO_4 experiment. This value accounts for the fractionation related to the formation of BT by elemental S/H_2S incorporation into n-C_{16} (2‰).

The results of the calculations for the $CaSO_4$ experiments do not fit the Rayleigh distillation model for $\alpha = 1.020$ (not shown) and $\alpha = 1.011$ (Fig. 8a,b).

However, Rayleigh distillation may be a reasonable model to explain the early stages of the Na_2SO_4 experiments using $\alpha = 1.011$, but not at the later stages (Fig. 8c). We therefore conclude that both the $CaSO_4$ and Na_2SO_4 systems are influenced by additional factors apart from closed-system distillation as is discussed below.

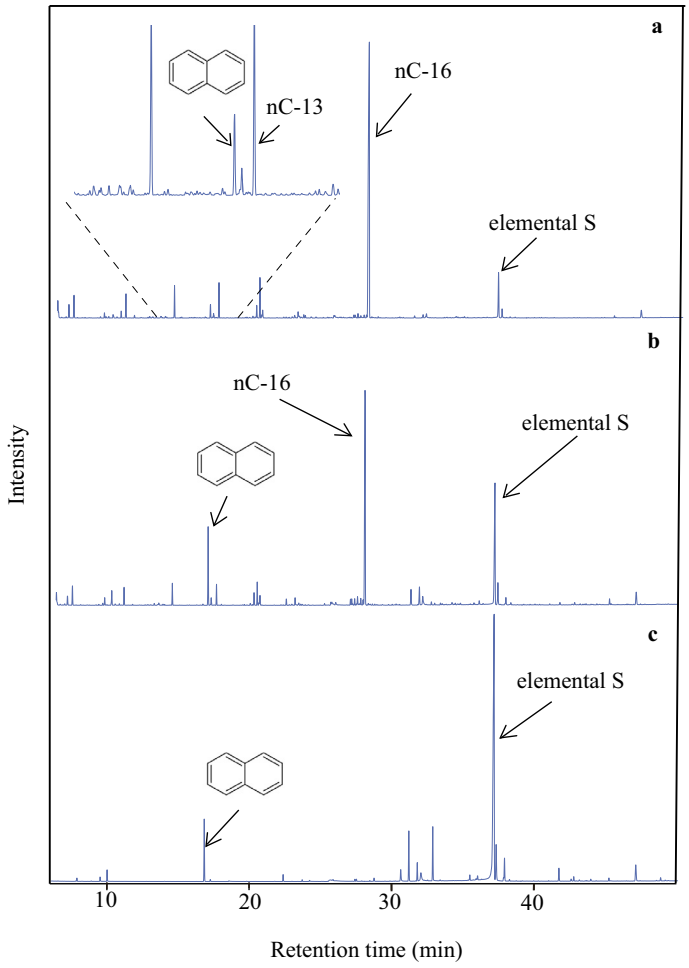

Fig. 5. GC–MS chromatograms of the 180 h experiments of the three TSR experiments (a) Limited $CaSO_4$, (b) Excess $CaSO_4$, (c) Excess Na_2SO_4.

4.1.4. $CaSO_4$ dissolution

The differences among some of the results observed for the $CaSO_4$ and Na_2SO_4 experiments can be explained by the slow dissolution rate of $CaSO_4$ under our experimental conditions. In both the "limited" and "excess" $CaSO_4$ experiments there is a large amount of solid-phase $CaSO_4$ present for most of the reaction times. Under the same experimental conditions, Na_2SO_4 is always fully soluble and thus immediately available for TSR. Indeed, for natural systems it has been suggested that the isotopic fractionation during TSR is largely controlled by the rate of dissolution of sulfate minerals, which can be slower than the rate of the dissolved sulfate consumption via reduction by organic molecules (Ohmoto and Rye, 1979; Powell and Macqueen, 1984; Machel et al., 1995). Therefore, dissolution of $CaSO_4$ may be the rate-limiting step in the reduction of sulfate during the TSR process in nature. Consequently, most reports of natural occurrences of TSR find minimal sulfur isotope fractionation among sulfate, hydrogen sulfide, and bulk oils (Krouse, 1977; Worden and Smalley, 1996; Cai et al., 2003).

The notion that sulfate dissolution rates affect apparent isotopic fractionations in natural occurrences of TSR is supported by the observations from the experiments performed in this study. The temperature, *p*H, and sulfate concentration all control the amount of reactive sulfate (HSO_4^-) available in solution in these experiments (Ma et al., 2008). The limited-$CaSO_4$ experiments initially contained 0.018 mmol of $CaSO_4$ in solution plus an additional 0.076 mmol of sulfate solid, for a total of 0.094 mmol of sulfate in the system (see Section 2). At this concentration, there is solid sulfate initially present in the experiments, and the rate of TSR is slow enough that sulfate dissolution does not limit the overall reaction process. In this case, significant sulfur isotopic fractionation is observed between the source sulfate and the generated H_2S and OSCs (Fig. 1c). However, once a certain portion of the soluble sulfate is consumed, the system starts to become sulfate limited and the apparent fractionation rapidly diminishes. This sulfate limitation begins to be apparent after about 20 h in the limited-$CaSO_4$ experiments.

The excess-$CaSO_4$ experiments initially contained 0.77 mmol of total sulfate (0.018 mmol in solution plus 0.75 mmol of solid sulfate, see Section 2 and Table 1), nearly one order of magnitude greater than in the limited experiments. At this high sulfate concentration, the rate

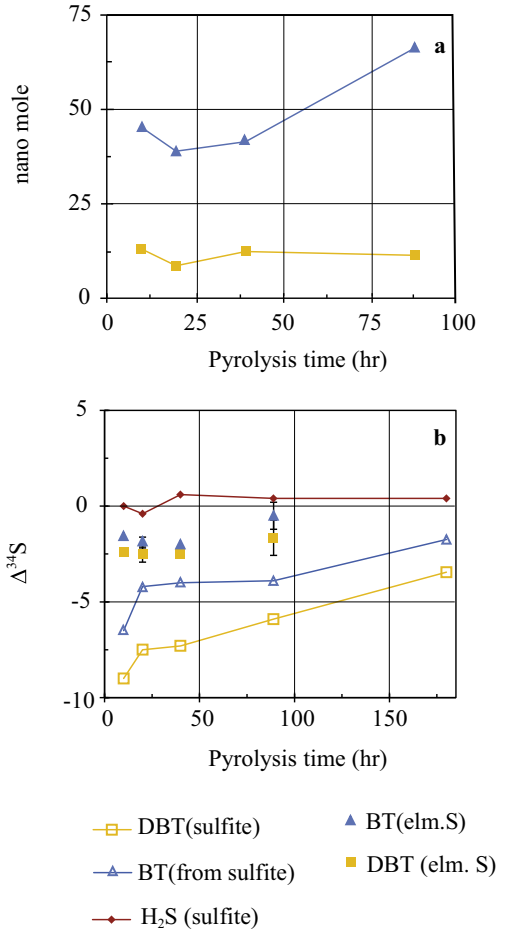

Fig. 6. Gold-tube pyrolysis experiments (360 °C). (a) Quantification of the elemental sulfur extracted OSCs. (b) Isotopic fractionation for both elemental S and Na_2SO_3 experiments. The results are normalized as fractionation from the initial S source Na_2SO_3 (−1.3‰) and elemental sulfur (1.2‰).

of TSR is expected to be commensurately faster. This is supported by the larger amount of H_2S generated and greater extent of sulfate reduction observed in the excess- versus limited-SO_4 experiments (Figs. 1a and 3a). In both the limited- and excess-sulfate experiments, OSCs show significant ^{34}S-depletion at the earliest stages of TSR, and then their $\delta^{34}S$ values increased rapidly and reached a plateau, 5–10‰ lower than the source sulfate (Fig. 3c). However, H_2S in the limited-sulfate experiment exhibited a similar isotopic pattern; whereas, the H_2S generated in the excess-sulfate experiments has a nearly constant $\delta^{34}S$ value that is equivalent to that of supplied sulfate, even in the earliest H_2S observation (20 h). This is explained by the significantly faster rate of TSR in the excess compared to the limited-sulfate experiments. At the lower total sulfate concentrations (limited $CaSO_4$), the TSR reactions in the short term experiments (<40 h) follow the slow, non-autocatalytic pathway. However, the excess-sulfate experiments contain a sufficiently large amount of reactive sulfate (HSO_4^-) that the fast, autocatalytic TSR reaction becomes dominant the pathway at a very early stage (<20 h). Consequently, the dissolved sulfate is rapidly consumed and the dissolution of solid sulfate becomes rate limiting, leading to no apparent S-isotope fractionation between sulfate and sulfide. The slow, non-autocatalytic TSR reaction can be inferred to have occurred in the very initial stages (<<20 h) of the excess sulfate experiments by the ^{34}S-depletion observed in the earliest measured OSCs. As discussed above (Section 4.1.2), such $\delta^{34}S$ values require a ^{34}S-depleted source, which can logically be assumed to be the H_2S generated from non-autocatalytic TSR.

The clearest evidence for the effect of sulfate solubility on S-isotope fractionation in TSR reactions is provided by comparison of the results of the sparingly soluble $CaSO_4$ experiments with those involving fully soluble Na_2SO_4 (Figs. 1c, 3c, and 4c). At the initial reaction times, the Na_2SO_4 experiments show fractionations between sulfate and OSCs similar to those observed in the $CaSO_4$ experiments. However, at the later reaction times the $\delta^{34}S$ values of the OSCs do not increase toward sulfate, but rather remain significantly depleted. Likewise, the H_2S generated by TSR reactions in the Na_2SO_4 experiments was consistently ^{34}S-depleted relative to the sulfate at all reaction times (Fig. 4c). The significant S-isotope fractionation observed in all of the TSR products generated in the Na_2SO_4 experiments lends unequivocal support to the notion that rate-limiting dissolution of solid sulfate in TSR reactions involving $CaSO_4$ can obscure the actual S isotope effects associated with sulfate reduction. This can explain the apparent lack of S-isotopic fractionation often observed in natural systems, and accounts for some of the deviation from Rayleigh distillation behavior observed in the experimental results of the present study.

4.1.5. Equilibrium isotope effects

In experiments with Na_2SO_4, the isotopic fractionation between H_2S and *residual* sulfate after 20 h was 13.4‰

Table 4
Results ($\delta^{34}S$ values) for the individual gold-tube pyrolysis experiments with elemental sulfur and *n*-C16.

	Initial elemental sulfur = 1.3‰			Initial elemental sulfur = 20.2‰		$\Delta^{34}S = \delta^{34}S$(product) − $\delta^{34}S$(initial sulfite)	
	Pyrolysis time (h)	BT (‰)	DBT (‰)	BT (‰)	DBT (‰)	$\Delta^{34}S$ BT (‰)	$\Delta^{34}S$ DBT (‰)
Elemental sulfur	10	–	–	18.6	17.8	−1.6	−2.4
	20	−0.4	−1.5	18.1	18.0	−1.9 ± 0.3	−2.5 ± 0.4
	40	–	–	18.2	17.7	−2.0	−2.5
	89	0.3	−1	20.2	19.2	−0.5 ± 0.7	−1.7 ± 0.9

Table 5
Results ($\delta^{34}S$ values) for the individual gold-tube pyrolysis experiments with Na_2SO_3 and *n*-C16.

Initial sodium sulfite (Na_2SO_3) = −1.3‰					$\Delta^{34}S = \delta^{34}S$(product) − $\delta^{34}S$(initial sulfite)		
	Pyrolysis time (h)	BT (‰)	DBT (‰)	H_2S (‰)	$\Delta^{34}S$ BT (‰)	$\Delta^{34}S$ DBT (‰)	$\Delta^{34}S$ H_2S (‰)
Na_2SO_3	10	−7.8	−10.3	−1.3	−6.5	−9.0	0.0
	20	−5.5	−8.8	−1.7	−4.2	−7.5	−0.4
	40	−5.3	−8.6	−0.7	−4.0	−7.3	0.6
	89	−5.2	−7.2	−0.9	−3.9	−5.9	0.4
	180	−3.0	−4.7	−0.9	−1.7	−3.4	0.4

and after 89 h of pyrolysis increased to 17.0‰ and 18.4‰ after 180 h (Fig. 4c and Table 3). Note that these fractionations were calculated based on the *residual* sulfate in the system after each experiment and not to the initial sulfate as presented in Table 3. This is because in the case of Na_2SO_4 experiments, the residual sulfate $\delta^{34}S$ values have changed significantly. The increase in the absolute magnitude of fractionation between H_2S and its source sulfate in the later reaction times is counterintuitive as one would expect the opposite trend.

The magnitude of fractionation at the later stages of the Na_2SO_4 experiments is similar to that reported by Ohmoto and Lasaga (1982). They suggested the following reaction scheme to explain the equilibrium isotopic effect (EIE) in hydrothermal sulfate-sulfide systems with no organic compounds present.

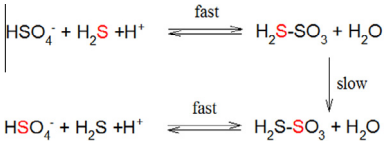

(8)

Ohmoto and Lasaga (1982) propose that the fractionation factor for this equilibrium is described by:

$$1000\ln(\alpha) = \frac{6.463 * 10^6}{(T)^2} + 0.56 \quad (9)$$

Using this equation, the fractionation between sulfate and sulfide predicted in our system would be 16.8‰, close to the range of fractionations (17.0 to 18.4‰) observed at the later reaction times (Fig. 4c). The chromatograms of the extractable residual organic matter in the Na_2SO_4 experiments reveal that *n*-C_{16} and other secondarily formed straight-chain hydrocarbons and single-ring aromatic compounds were completely consumed (Fig. 5c). Moreover, elemental S became more dominant in the chromatogram of the Na_2SO_4 experiments providing additional support for the absence of sufficient oxidizable hydrocarbons (Fig. 5). This indicates that the main reactive hydrocarbons for the TSR reaction were absent at these reaction times. However, in the $CaSO_4$ experiments abundant *n*-C_{16} remained throughout all stages of the reaction (i.e., it was not completely consumed). These observations, combined with the low consumption of sulfate at this stage and the very minor increase in H_2S concentration suggests that the TSR reaction has stopped or become very slow (Fig. 4a). Therefore the system at this stage, with no hydrocarbons to react with sulfate, is similar to the system described by Ohmoto and Lasaga (1982) and exhibiting a similar EIE between sulfate and sulfide.

We suggest that the fractionations measured in the Na_2SO_4 experimental system were governed by both kinetic and equilibrium isotope effects at different stages. When reactive organic compounds are abundant in the system, sulfate reduction is occurring and the dominant fractionation mechanism is kinetic. When the sulfate reduction has slowed down or stopped, equilibrium is attained between sulfate and sulfide and the isotopic fractionation is governed by equilibrium effects. This can also explain why the Rayleigh distillation model was able to fit the early stages of TSR in the Na_2SO_4 experiments, but did not accurately predict S-isotopic compositions of the TSR products at the later stages (>40 h) when TSR had significantly slowed or stopped.

4.2. Isotope fractionation during OSC formation

4.2.1. Relative reaction rates and $\delta^{34}S$ values of OSCs

In the $CaSO_4$ experiments, the initial large S-isotope fractionation between OSCs (BT and DBT) and the source sulfate rapidly disappears and the $\delta^{34}S$ values converge to that of H_2S and sulfate (Figs. 1c and 3c). However, the rates of the convergence differ with BT $\delta^{34}S$ changing faster than that of DBT. BT degrades faster than DBT during all experiments because of its lower thermal stability. Another possible reason for the change in the relative abundance of BT and DBT is a decrease in the respective formation rates as a result of the limited availability of suitable precursor compounds. Aromatic precursors (e.g., alkyl-benzenes) are known to react with sulfur at elevated temperatures and produce BTs, while fused aromatic rings and biphenyls produce DBTs (Aizenshtat et al., 1995; Asif et al., 2009). With increasing thermal maturation and TSR, there are more fused aromatic compounds present and consequently more opportunities for DBT formation than BT (Radke et al., 1982). At every reaction time, the concentrations of BT and DBT are controlled by their relative formation and degradation rates.

No significant S-isotope fractionation is apparent during the thermal degradation of either BT or DBT. In the excess-$CaSO_4$ experiments, the BT concentration from 89 to 180 h decreases by nearly 80% while its $\delta^{34}S$ composition changes by <1.5‰ (Figs. 1b and 3b). In the Na_2SO_4 experiments, a drop in the DBT concentration from 354 to

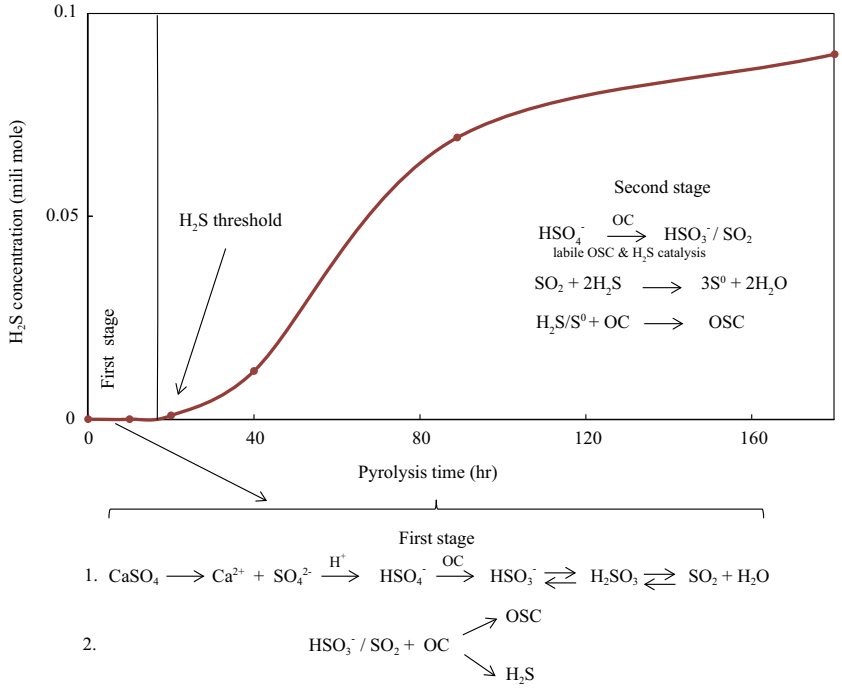

Fig. 7. The suggested two stages of TSR reaction and their associated chemical reactions as deduced from our experimental results.

153 nmol is accompanied by no change in the $\delta^{34}S$ (Figs. 4b and 4c). The steady-state $\delta^{34}S$ of BT and DBT is controlled by the balance of isotope effects on synthesis and degradation. Our data are consistent with little fractionation on degradation, but we cannot prove it is zero. We hypothesize that the steady-state values are therefore mainly controlled by fractionations during synthesis, which should reflect the reactive inorganic S species. The newly formed OSCs carry the $\delta^{34}S$ value of the reduced inorganic S species (e.g., H_2S produced during TSR) as evidenced by the experiments with elemental S (Fig. 6b). In the experiments with $CaSO_4$, the H_2S converges to the $\delta^{34}S$ value of the source sulfate very quickly (0–20 h). The $\delta^{34}S$ value of OSC at any given reaction time will be the result of a mixture of early formed OSC that has ^{34}S-depleted values and newly formed OSC with relatively ^{34}S-enriched values inherited from the inorganic reduced S species produced by TSR at each step. The degree of mixing of sources will be determined by the residence time of BT and DBT in the system, which in turn is related to the relative thermal degradation rate as well as the formation rate during these experiments.

4.2.2. Sulfur sources for OSCs during TSR

Significant quantities of OSCs are known to be formed via reactions of reduced S species with petroleum hydrocarbons during TSR. Hydrogen sulfide is generally assumed to be the predominant species that forms OSCs, because of its high abundance relative to all other reduced S species in petroleum reservoirs (Orr, 1974; Powell and Macqueen, 1984; Hanin et al., 2002; Cai et al., 2003, 2009).

However, other possible S sources for OSC formation during TSR may be intermediate oxidation-state S species such as elemental S, S_x^{-2}, SO_3^{-2}, and $S_2O_3^{-2}$ (Goldstein and Aizenshtat, 1994). These intermediate S species readily react with hydrocarbons to form OSC, and H_2S is also formed either through direct reduction of the intermediate S or by subsequent thermal cracking of the OSC (Aizenshtat et al., 1995; Lewan, 1998). A recent study has shown that tri-sulfur ions (S_3^-) are formed during heating experiments of aqueous sulfate solutions, suggesting that this may be an important intermediate in the reduction of sulfate (Truche et al., 2014). The mechanism for S_3^- ion formation is unknown; however, once formed it can be reduced in the presence of protons to sulfide or form thiophenes, although this was shown only under basic conditions (Zhang et al., 2015). If the reaction of S_3^- or other intermediate S species with organic compounds have S-isotopic fractionations distinct from that of H_2S-HC this would be expected to be recorded in the $\delta^{34}S$ values of the OSCs. At this stage we cannot examine the role of S_3^- in TSR and its possible S-isotopic signature, because we cannot produce or purchase S_3^- reagent. We therefore examined two model compounds (elemental S and sulfite) of different oxidation states (0 and +4) to be representative of intermediate and reduced S species. The experiments with elemental S and C_{16} yielded relatively small fractionation of the newly formed OSCs, while the experiments with sulfite have very distinct fractionations (up to 9.0‰) at the early stages of the reaction (Fig. 6b).

Sulfite is likely to react with organic molecules at the earliest stages of TSR, because this species forms immediately after the cleavage of the first S–O bond in sulfate, which is required for the TSR reaction (Ma et al., 2008). This first S–O bond cleavage of sulfate was suggested as the rate-limiting step in TSR leading to the formation of

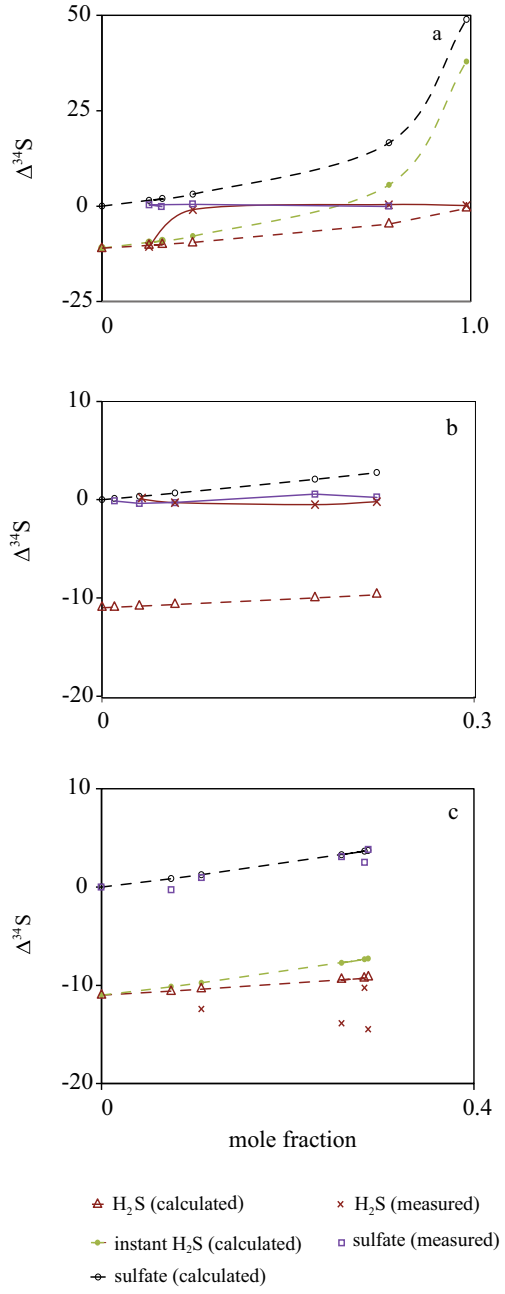

Fig. 8. Closed-system (Rayleigh) distillation calculations for the three TSR pyrolysis experiments. The calculated and measured fractionation between sulfate and H_2S. Measured sulfate consumption was used to calculate f based on the assumption that it was fully converted to H_2S and assuming $\alpha = -11‰$ (a) The $CaSO_4$ limited experiments (b) The $CaSO_4$ excess experiments (c) The Na_2SO_4 experiments.

^{34}S-depleted sulfite (SO_3^{-2}) via a KIE (Harrison and Thode, 1957; Kiyosu, 1980).

Sulfite is highly reactive with organic compounds, and can be quickly reduced to the S^{2-} oxidation state (Fig. 7), as is evident in the present experiments with n-C_{16} and Na_2SO_3 and in a previous study in which SO_3^{2-} was completely consumed in <20 h and yielded H_2S (Amrani et al., 2008). Therefore, only the initial reaction time (10 h) may uniquely represent the S-isotope fractionation associated with the formation of OSCs from the reaction of sulfite and organic compounds at our experimental conditions (first stage, Fig. 7). The fractionation in the Na_2SO_3 experiments is initially as large as 9.0‰ (Fig. 6b). The details of the mechanism of SO_3^{2-} reaction with hydrocarbons at elevated temperatures is not well understood, but it likely involves reactions with SO_2, which has the same oxidation state as SO_3^{2-} and may attain equilibrium with it under our experimental conditions (Fig. 7).

As the reaction progresses, the $\delta^{34}S$ of the OSCs quickly become ^{34}S-enriched and we hypothesize that the dominant reaction in the system shifts from $SO_3^{2-} + n$-C_{16} to H_2S + n-C_{16}, with a much smaller fractionation in the range of 1–3‰ (Fig. 6a). When SO_2 and H_2S are present they can form elemental sulfur (Drozdova and Steudel, 1995 and references therein) which at elevated temperatures (similar to our system) will form highly reactive polysulfides that can readily react with organic matter to form OSC (Goldstein and Aizenshtat, 1994). As seen from the elemental sulfur experiments the OSCs formed by this reaction are only 1–3‰ ^{34}S-depleted relative to their source elemental S (Fig. 6b). The reduction of SO_3^{2-} to H_2S has minimal apparent fractionation associated with it, as is evident in our experiments starting with Na_2SO_3 (Fig. 6b). This is thought to result from rapid equilibration among all intermediate (or reduced) S species present, and the fact that most of the sulfite is reduced within the first few hours of the experiments. The ^{34}S-enriched OSCs generated at later reaction stages (>20 h) mix with the early ^{34}S-depleted OSCs, causing $\delta^{34}S$ values of the bulk OSCs to gradually converge to the composition of the initial sulfite (Fig. 6b). We therefore conclude that the formation of OSCs via SO_3^{2-} reduction by hydrocarbons is accompanied by a significant S-isotope fractionation in the range of ~10‰. We propose that this relatively large fractionation explains the large ^{34}S depletions recorded by OSCs and H_2S during the initial stages of our TSR experiments (Figs. 1, 3, 4 and 7).

4.3. S-isotope fractionations throughout the TSR process

Based on differences in reaction rates and availability of reactants, a multi-stage model of the overall TSR process has been proposed that involves distinct reaction mechanisms at different stages of TSR (Zhang et al., 2008, 2012; Xia et al., 2014). If reaction mechanisms vary over the duration of TSR, it is reasonable to expect that these could be reflected in distinct S-isotopic fractionations throughout the TSR process, as presented in Fig. 7. The $\delta^{34}S$ composition of the initial and generated S-containing species in the present experimental work can be used to evaluate this proposition (Fig. 9). The results from the experiments containing Na_2SO_4 are best suited for this task because there is no limitation on the availability of sulfate (as in the limited-$CaSO_4$ experiments) nor complication from sulfate dissolution, which can obscure the reaction-specific fractionations (Fig. 3c). In the first non-catalytic stage of TSR (0–20 h), the formation of OSCs associated with HSO_4^- reduction is accompanied by significant isotopic fractionation that

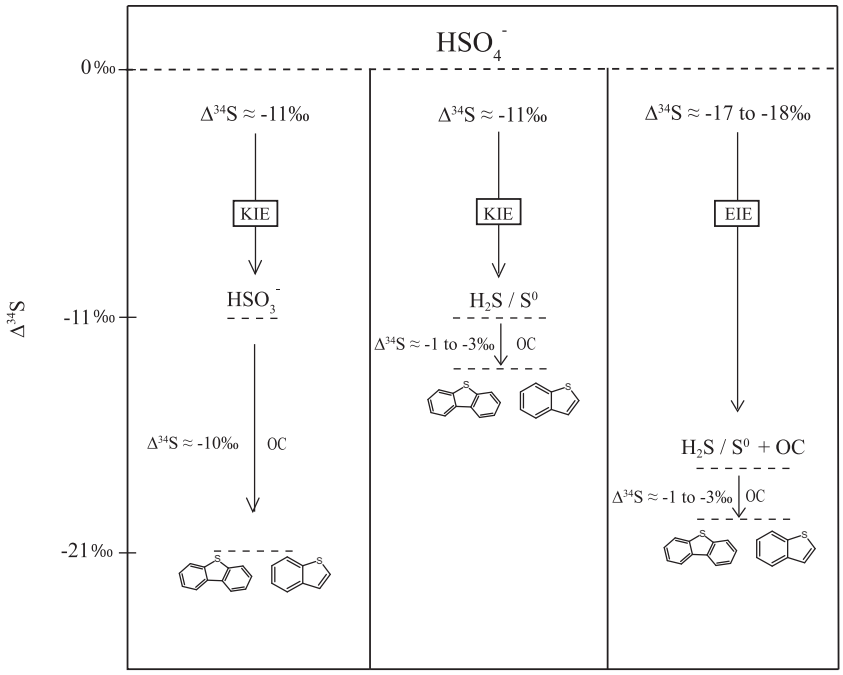

Fig. 9. Scheme of the different fractionations observed in our experiments and the different mechanisms that are associated with them based on kinetic isotope effect (KIE) and equilibrium isotope effect (EIE).

reaches values as great as 22.2‰ as recorded in BT (Fig. 4c). The maximum fractionation observed for H_2S generated during this initial stage of TSR is 12.4‰. This value is close to that reported by Kiyosu (1980) (8–10‰) for the kinetic isotopic fractionation for sulfate reduced to sulfide.

At 20 h reaction time, the difference between the $\delta^{34}S$ of BT and H_2S has dropped to 4.7‰ (Fig. 4c). This difference between H_2S and the coexisting BT is larger than expected for fractionation related to the formation of OSCs from H_2S or elemental S. Therefore, it can be inferred that other S species are more important in the formation of OSCs during the initial non-catalytic phase of TSR. The fractionation of 4.7‰ observed in the early stages of the Na_2SO_4 experiments is identical within analytical uncertainties to that recorded in the SO_3^{2-} experiments (4.3‰, Fig. 6b), suggesting that SO_3^{2-} rather than H_2S is the S source for OSC formation at reactions times of 20 h. This finding is consistent with the work of Kiyosu and Krouse (1990) who observed a 4–5‰ fractionation for sulfate reduced to sulfur in an intermediate oxidation state prior to reduction to sulfide.

This may suggest that the observed fractionation in OSCs formed during the initial phase of TSR (~20‰) is the net result of two major reactions: first, the reduction of SO_4^{2-} to SO_3^{2-} (S^{+6} to S^{+4}), which is the rate-limiting step for TSR and is shown (above) to have a fractionation of 11 to 12‰; and second, the fractionation associated with the formation of OSC from hydrocarbons reacted with the ^{34}S-depleted SO_3^{2-} (~10‰; Figs. 6b and 9). The results of all three sets of sulfate reduction experiments (limited- and excess-$CaSO_4$ and Na_2SO_4) show overall fractionations between initial sulfate and generated OSCs at the initial stage of TSR that are consistent with this composite fractionation (Figs. 1c, 3c and 4c). This mechanism can also potentially explain the large differences in the $\delta^{34}S$ of OSCs and coexisting H_2S at the earliest stage of TSR, and shows that the results of the present study are consistent with the earlier findings of both Kiyosu (1980) and Kiyosu and Krouse (1990).

During the second catalytic stage of TSR, when much greater amounts of H_2S are present, organic compounds are more likely to react with H_2S than with the SO_3^{2-} (or SO_2) produced from the reduction of sulfate. This is because the concentration of H_2S is much higher than that of the less stable and short-lived SO_3^{2-}. Similarly, as TSR progresses, SO_3^{2-} (or SO_2) has increasing probability of reacting with H_2S rather than (or at least, in addition to) organic compounds, producing elemental S according to the following reaction (Eq. (10) and Fig. 7):

$$SO_2 + 2H_2S \rightarrow 3S + 2H_2O \quad (10)$$

This process yields elemental S that can then react with hydrocarbons to form OSCs with a small fractionation of ~1–3‰ (Fig. 6b). Furthermore, cracking of thermally labile OSCs releases H_2S that can further react with hydrocarbons or SO_2 leading to homogenization of the S-isotope pool among all organic and inorganic S species. Fig. 9 summarizes the isotopic fractionations during the different TSR stages as we propose.

4.4. Geochemical implications

The S-isotopic results presented herein are consistent with a multi-stage reaction mechanism for the overall TSR process as previously proposed (Zhang et al., 2008, 2012; Xia et al., 2014). The initial non-catalytic stage of TSR involves the reduction of sulfate to sulfite at a slow

rate. The OSCs formed during the earliest portion of this stage have distinctive, low $\delta^{34}S$ values due to their formation by reduction of sulfite. The progression of the initial phase of TSR is reflected in the gradual ^{34}S-enrichment in the OSCs as new molecules are generated from reactions of hydrocarbons with sulfur in lower oxidation states (e.g., S°, H_2S). It has been suggested that the breaking of S–O bonds in aqueous sulfate ions during the first step of sulfate reduction is the rate-limiting step in the overall TSR process (Harrison and Thode, 1957; Kiyosu, 1980; Ma et al., 2008). However, the results of the present study show that other factors such as the availability of reactants (e.g., sulfate dissolution) can be rate-limiting during TSR. More accurately, the initial reduction of sulfate to sulfite controls the onset of the overall TSR process. The rate of sulfate reduction significantly increases during the second, autocatalytic phase of TSR as shown in previous studies (Amrani et al., 2008; Zhang et al., 2008, 2012) and confirmed by the present experimental results. This stage of TSR is clearly identified by the rapid convergence of the $\delta^{34}S$ values of the generated H_2S and OSCs toward that of the supplied sulfate. TSR experiments involving sparingly soluble $CaSO_4$ confirm field observations (Orr, 1974; Machel, 2001) that the rate of sulfate reduction can be sufficiently rapid such that sulfate dissolution becomes the rate-limiting step in the overall TSR process. In these instances, no S-isotopic fractionation is observed between generated sulfide and source sulfate.

The $\delta^{34}S$ values obtained in the present study provide supporting evidence for the interpretation of the sulfur isotopic composition of individual OSCs in natural crude oils. Recent studies of oils from the Smackover Formation that had been exposed to TSR found S-isotopic differences as great as 30‰ between BT and DBT within individual oil samples (Amrani et al., 2012; Gvirtzman et al., 2015). Amrani et al. (2012) suggested that the $\delta^{34}S$ values of BTs and DBTs in TSR-affected oils are controlled by the S-isotopic composition of the reduced S source, and differences in the relative thermal stabilities of the compounds. Extreme differences between the $\delta^{34}S$ values of BTs and DBTs are explained by the fact that BTs are very reactive and quickly assimilate the isotopic composition of the reduced sulfur source (i.e., H_2S); whereas, the DBTs are more refractory and retain the $\delta^{34}S$ value of the kerogen source longer (Amrani et al., 2012). This interpretation is predicated on the assumptions that (1) fractionation associated with the formation of OSCs (e.g., BTs and DBTs) from the reaction of reduced S species such as H_2S with organic compounds is minor (Amrani, 2014), and (2) fractionations during the formation of individual OSCs (e.g., BT and DBT) are similar at the same temperature.

The present study provides experimental evidence that supports these interpretations, and provides additional insights into the details of the reaction mechanisms. Specifically, the fractionation between reduced S sources (e.g., elemental S) and generated OSCs is relatively small (<4‰); however, OSCs generated in association with the reduction of more oxidized sulfur species (i.e., SO_4^{2-} and SO_3^{2-}) have significantly larger S-isotopic fractionations. Consequently, the $\delta^{34}S$ of individual OSCs can be traced to the S source (e.g., SO_3^{2-} versus H_2S) providing a sensitive tool for assessing the extent of TSR that an oil has experienced, particularly during the first and early part of the second stage of TSR. Moreover, the residence time of these molecules in the system–and thus the rate at which the $\delta^{34}S$ values of OSC adjust towards those of new sources (e.g., SO_4^{2-})–is dependent on the thermal stability of the molecules. For example, in Smackover oils exposed to variable amounts of TSR, the $\delta^{34}S$ values of BTs increase much more quickly than those of DBTs (Amrani et al., 2012).

The sulfur isotopic compositions of individual organosulfur compounds in natural crude oils has the potential to provide critical information that cannot be determined from $\delta^{34}S$ of bulk phases alone (e.g., whole oil, sulfate minerals, and H_2S). However, the accurate interpretation of molecular-level results in complex mixtures, such as natural crude oils, requires controlled experimental studies to identify the factors responsible for producing these isotopic signatures. The present study provides some insights into the primary controls on the $\delta^{34}S$ values of OSCs in petroleum exposed to TSR. These values can offer diagnostic information on the extent of TSR that has occurred in a reservoir, as well as help to refine and constrain predictive models of TSR occurrence. It should be noted though, that extrapolation of high-temperature, short-term experimental results to low-temperature, long-term reactions that occur in natural environments must be made cautiously. Further work is needed to fully understand the effects of TSR on the S-isotopic composition of individual OSCs in petroleum.

5. CONCLUSIONS

The main conclusions from this study are:

1. The observed S-isotopic fractionations between sulfate and BT, DBT, and H_2S in experimental simulations of TSR correlate well with the two-stage model (Zhang et al., 2008) of the overall TSR process. This fractionation decreases as the H_2S concentration increases and the reaction enters the second, catalyzed stage, indicating that different reaction mechanisms are involved in these two distinct stages of TSR.
2. Under the experimental conditions studied, the maximum fractionations observed for H_2S and OSC generated during the initial stage of TSR are 12.4‰ and 22.2‰, respectively.
3. OSCs produced from the reaction of *n*-C_{16} with elemental S have S-isotopic fractionations in the range of 0.5 to 4‰, and show little variation over all reaction times. Similar experiments with sulfite (Na_2SO_3) instead of elemental S show initial fractionations as large as 9.0‰ that rapidly disappear with progressive reaction time. In both cases (SO_3^{2-} and S°), the coexisting H_2S has $\delta^{34}S$ values similar to the initial S source.
4. There is S-isotopic evidence for the involvement of SO_3^{2-} as an intermediary in the early uncatalyzed stage of TSR.
5. The $\delta^{34}S$ compositions of the OSCs 2-PT, BT and DBT exhibit different responses as TSR progresses in the experimental systems studied. The observed fractionation

between the individual OSCs and the coexisting H_2S correlates with the respective thermal stabilities of the OSCs. DBT is the most thermally stable and the slowest to adopt the $\delta^{34}S$ value of the coexisting H_2S throughout the TSR process, whereas 2-PT is the least stable and fastest to incorporate the $\delta^{34}S$ value of H_2S.

6. The aqueous solubility of $CaSO_4$ can be a limiting factor that controls the S-isotopic fractionation between sulfate and sulfide during TSR. This supports the notion that $CaSO_4$ dissolution can lead to the apparent lack of fractionation between sulfate and sulfide produced by TSR in nature.
7. $\delta^{34}S$ values of the products of the early stages of the TSR experiments involving Na_2SO_4 are governed by the KIE, whereas EIE is observed at later stages once all of the readily oxidizable hydrocarbons have been consumed.
8. The S-isotopic composition of individual OSCs record information related to geochemical reactions that cannot be discerned from the $\delta^{34}S$ values obtained from bulk phases such as H_2S, oil, and sulfate minerals, which can provide important mechanistic details about the overall TSR process.

ACKNOWLEDGMENTS

Alexander Meshoulam thanks the Ministry of National Infrastructures Energy and Water Resources of Israel for MSc grant. Alon Amrani thanks the Israeli Science Foundation (ISF) Grant Number 1269/12 for partial support of this study. Liu Jinzhong acknowledge the support by the Chinese National Scientific Foundation number 41173069 and 41321001. We are also thank Gilad Antler (Cambridge University, UK) for bulk S analysis of some of the starting materials for interlaboratory comparison. We also grateful to Li Gao (PEERI), Bob Dias (U. S. Geological Survey) and three anonymous referees for helpful comments on an earlier version of this manuscript. Any use of trade, product, or firm names is for descriptive purposes only and does not imply endorsement by the U.S. Government.

REFERENCES

Aizenshtat Z., Krein E. B., Vairavamurthy M. A. and Goldstein T. P. (1995) Role of sulfur in the transformation of sedimentary organic matter: a mechanistic overview. *Am. Chem. Soc.* **612**, 16–39.

Amrani A. (2014) Organosulfur compounds: Molecular and isotopic evolution from biota to oil and gas. *Annu. Rev. Earth Planet. Sci.* **42**, 733–768.

Amrani A., Said-Ahamed W., Lewan M. D. and Aizenshtat Z. (2006) Experiments on $\delta^{34}S$ mixing between organic and inorganic sulfur species during thermal maturation. *Geochim. Cosmochim. Acta* **70**, 5146–5161.

Amrani A., Zhang T., Ma Q., Ellis G. S. and Tang Y. (2008) The role of labile sulfur compounds in thermochemical sulfate reduction. *Geochim. Cosmochim. Acta* **72**(2008), 2960–2972.

Amrani A., Sessions A. L. and Adkins J. F. (2009) Compound-specific delta S-34 analysis of volatile organics by coupled GC/multicollector-ICPMS. *Anal. Chem.* **81**(21), 9027–9034.

Amrani A., Deev A., Sessions A. L., Tang Y., Adkins J. F., Hill R. J., Moldowan J. M. and Wei Z. (2012) The sulfur-isotopic compositions of benzothiophenes and dibenzothiophenes as a proxy for thermochemical sulfate reduction. *Geochim. Cosmochim. Acta* **84**, 152–164.

Asif M., Alexander R., Faseelat T. and Pierce K. (2009) Geosynthesis of dibenzothiophene and alkyl dibenzothiophene in crude oil and sediments by carbon catalysis. *Org. Geochem.* **40**(8), 895–901.

Cai C. F., Worden R. H., Bottrell S. H., Wang L. S. and Yang C. C. (2003) Thermochemical sulphate reduction and the generation of hydrogen sulphide and thiols (mercaptans) in Triassic carbonate reservoirs from the Sichuan Basin, China. *Chem. Geol* **202**(1–2), 39.

Cai C. F., Zhang C. M., Cai L. L., Wu G. H., Jiang L., Xu Z. M., Li K. K., Ma A. L. and Chen L. X. (2009) Origins of Paleozoic oils in the Tarim Basin: evidence from sulfur isotopes and biomarkers. *Chem. Geol.* **268**(3–4), 197–210.

Cai C. F., Amrani A., Worden R. H., Xiao Q., Wang T., Gvirtzman Z., Li H., Said-Ahmad W. and Jia L. (2016) The sulfur isotopic compositions of individual sulfur compounds and their genetic link in the Lower Paleozoic petroleum pools of the Tarim Basin, NW China. *Geochim. Cosmochim Acta* **182**, 88–108.

Cross M. M., Manning D. A. C., Bottrell S. H. and Worden R. H. (2004) Thermochemical sulphate reduction (TSR): experimental determination of reaction kinetics and implications of the observed reaction rates for petroleum reservoirs. *Org. Geochem.* **35**, 393–404.

Drozdova Y. and Steudel R. (1995) The reaction of H_2S with SO_2—molecular structures, energies, and vibrational data of 7 isomeric forms of H_2S_3O. *Chem. Eur. J.* **1**, 193–198.

Goldhaber M. B. and Orr W. L. (1995) Kinetic controls on thermochemical sulfate reduction as a source of sedimentary H_2S. In *Geochemical transformation of sedimentary sulfur*, vol. 612 (eds. M. A. Vairavamurthy and M. A. A. Schoonen), pp. 412–425. ACS Symposium Series.

Goldstein T. P. and Aizenshtat Z. (1994) Thermochemical sulfate reduction – a review. *J. Therm. Anal.* **42**(1), 241–290.

Greenwood P. F., Amrani A., Sessions A., Raven M. R., Holman A. L., Dror G., Grice K., McCulloch M. T. and Adkins J. F. (2014) Development and initial biogeochemical applications of compound-specific $\delta^{34}S$ analysis. In *RSC Detection Sciences Series No.4: Principles and practice of analytical Techniques in Geosciences* (ed. K. Grice). Royal Society of Chemistry, Oxford, pp. 285–312.

Grinenko V. A., Grinenko L. N. and Zagryazhskaya G. D. (1969) Kinetic isotope effect in high temperature reduction of sulfate. *Geokhimya* **4**, 484–491.

Gvirtzman Z., Said-Ahmad W., Ellis G. S., Hill R. J., Moldowan J. M., Wei Z. and Amrani A. (2015) Compound-specific sulfur isotope analysis of thiadiamondoids of oils from the Smackover Formation, USA. *Geochim. Cosmochim. Acta* **167**, 144–161.

Hanin S., Adam P., Kowalewski I., Huc A. Y., Carpentier B. and Albrecht P. (2002) Bridgehead alkylated 2-thiaadamantanes: novel markers for sulfurization processes occurring under high thermal stress in deep petroleum reservoirs. *Chem. Commun.* **16**, 1750–1751.

Harrison A. G. and Thode H. G. (1957) The kinetic isotope effect in the chemical reduction of sulphate. *Trans Farad. Soc.* **53**, 1648–1651.

Heydari E. and Moore C. H. (1989) Burial diagenesis and thermochemical sulfate reduction, Smackover Formation, southeastern Mississippi Salt Basin. *Geology* **17**, 1080–1084.

Kiyosu Y. (1980) Chemical reduction and sulfur isotope effects of sulfate by organic matter under hydrothermal conditions. *Chem. Geol.* **30**, 47–56.

Kiyosu Y. and Krouse H. R. (1990) The role of organic acid in the abiogenic reduction of sulfate and the sulfur isotope effect. *Geochem. J.* **24**, 21–27.

Kiyosu Y. and Krouse H. R. (1993) Thermochemical reduction and sulfur isotopic behavior of sulfate by acetic-acid in the presence of native sulfur. *Geochem. J.* **27**(1), 49.

Krouse H. R. (1977) Sulfur isotope studies and their role in petroleum exploration. *J. Geochem. Expl.* **7**(2), 189–211.

Lewan, M.D., (1998) Sulphur-radical control on petroleum formation rates. Nature 391(6663), 164 (199.

Ma Q., Ellis G. S., Amrani A., Zhang T. and Tang Y. (2008) Theoretical study on the reactivity of sulfate species with hydrocarbons. *Geochim. Cosmochim. Acta* **72**(2008), 4565–4576.

Machel H. G. (1987) Some aspects of diagenetic sulphate-hydrocarbon redox reactions. In *Diagenesis of Sedimentary Sequences*, vol. 36 (ed. J. D. Marshall). Geol. Soc. Spec. Publ, pp. 15±28.

Machel H. G., Krouse H. R. and Sassen R. (1995) Products and distinguishing criteria of bacterial and thermochemical sulfate reduction. *App. Geochem.* **10**(4), 373–389.

Machel H. G. (2001) Bacterial and thermochemical sulfate reduction in diagenetic settings – old and new insights. *Sed. Geol.* **140** (1–2), 143–175.

Oduro H., Harms B., Sintim H. O., Kaufman A. J., Cody G. and Farquhar J. (2011) Evidence of magnetic isotope effects during thermochemical sulfate reduction. *Proc. Natl. Acad. Sci. U.S.A.* **108**(43), 17635–17638.

Ohmoto H. and Rye R. O. (1979) Isotopes of sulfur and carbon. In *Geochemistry of hydrothermal Ore deposits*, Second ed. John Wiley and sons, New York, pp. 509–567, Chapter 10.

Ohmoto H. and Lasaga A. (1982) Kinetic of reaction between aqueous sulfate and sulfide in hydrothermal systems. *Geochem. Cosmochim Acta* **46**, 1727–1745.

Orr W. L. (1974) Changes in sulfur content and isotopic-ratios of sulfur during petroleum maturation – study of big horn basin paleozoic oils. *AAPG Bull.* **58**(11), 2295–2318.

Radke M., Welte D. H. and Willsch H. (1982) Geochemical study on a well in the Western Canada Basin: relation of the aromatic distribution pattern to maturity of organic matter. *Geochim. Cosmochim. Acta* **46**, 1–10.

Ricci M. P., Merritt D. A., Freeman K. H. and Hayes J. W. (1994) Acquisition and processing of data for isotope-ratio-monitoring mass spectrometry. *Org. Geochem.* **21**, 561–571.

Powell T. G. and Macqueen R. W. (1984) Precipitation of sulfide ores and organic matter – sulfate reactions at pine point, Canada. *Science* **224**(4644), 63–66.

Saccocia P. J. and Seyfried W. E. (1990) Talc-quartz equilibria and the stability of magnesium-chloride complexes in NaCl-$MgCl_2$ solutions at 300 °C, 350 °C and 400 °C, 500bars. *Geochim. Cosmochim. Acta* **54**(12), 3283–3294.

Said-Ahmad W. and Amrani A. (2013) A method for the sulfur isotope analysis of DMS and DMSP in seawater. *Rapid Commun. Mass Spectrom.* **27**, 2789–2796.

Sessions A. L., Burgoyne T. W. and Hayes J. M. (2001) Determination of the H_3 factor in hydrogen isotope ratio monitoring mass spectrometry. *Anal. Chem.* **73**, 200–207.

Seewald J. S., Eglinton L. B. and Ong Y. L. (2000) An experimental study of organic–inorganic interactions during vitrinite maturation. *Geochim. Cosmochim. Acta* **64**(9), 1577–1591.

Toland W. G. (1960) Oxidation of organic compounds with aqueous sulfate. *J. Am. Chem. Soc.* **82**, 1911–1916.

Truche L., Bazarkina E. F., Barré G., Thomassot E., Berger G., Dubessy J. and Robert P. (2014) The role of S_3^- ion in thermochemical sulfate reduction: geological and geochemical implications. *Earth Planet. Sci. Lett.* **396**, 190–200.

Watanabe Y., Farquhar J. and Ohmoto H. (2009) Anomalous fractionations of sulfur isotopes during thermo chemical sulfate reduction. *Science* **324**(5925), 370–373.

Wei Z., Moldowan J. M., Fago F., Dahl J. E., Cai C. and Peters K. E. (2007) Origins of thiadiamondoids and diamondoidthiols in petroleum. *Energ. Fuel.* **21**, 3431–3436.

Worden R. H., Smalley P. C. and Oxtoby N. H. (1995) Gas souring by thermochemical sulfate reduction at 140 °C. *Am. Assoc. Petrol. Geol. Bull.* **79**(6), 854–863.

Worden R. H. and Smalley P. C. (1996) H_2S-producing reactions in deep carbonate gas reservoirs: Khuff formation, Abu Dhabi. *Chem. Geol.* **133**(1–4), 157–171.

Worden R. H. and Smalley P. C. (2001) H2S in North Sea oil fields: importance of thermochemical sulphate reduction in clastic reservoirs. In *10th International Symposium on Water-Rock Interactions, 2* (ed. R. Cidu). Swets and Zeitlinger, Lisse, pp. 659–662.

Xia X., Ellis G. S., Ma Q. and Tang Y. (2014) Compositional and stable carbon isotopic fractionation during non-autocatalytic thermochemical sulfate reduction by gaseous hydrocarbons. *Geochim. Cosmochim. Acta* **13**, 472–486.

Zhang T., Amrani A., Ellis G. S., Ma Q. and Tang Y. (2008) Experimental investigation on thermochemical sulfate reduction by H_2S initiation. *Geochim. Cosmochim. Acta* **72**(2008), 3518–3530.

Zhang T., Ellis G. S., Ma Q., Amrani A. and Tang Y. (2012) Kinetics of uncatalyzed thermochemical sulfate reduction by sulfur-free paraffin. *Geochim. Cosmochim. Acta* **96**, 1–17.

Zhang G., Yi H., Chen H., Bian C., Liu C. and Lei A. (2015) Trisulfur radical anion as the key intermediate for the synthesis of thiophenes via the interaction between elemental sulfur and NaOBu. *Org. Lett.* **16**(23), 6156–6159.

Associate editor: Josef P. Werne